Punching Shear Behavior of UHPC Flat Slabs

Dissertation for the acquisition of the academic degree

Doktor der Ingenieurwissenschaften (Dr.-Ing.)

Submitted to the Faculty of Civil and Environmental Engineering of the University of Kassel

By Hussein Abbas Azeez Al-Quraishi

This work originated at the Institute of Structural Engineering in The Department of Civil and Environmental Engineering at the University of Kassel for obtaining the academic degree of Doctor of Engineering (Dr.-Ing.).

Approved dissertation.
First Supervisor: Prof. Dr.-Ing. Ekkehard Fehling
Second Supervisor: Prof. Dr.-Ing. Matthias Baitsch

Date of examination: 08. September 2014

Preface of Author

I dedicate this dissertation to the soul of Fatimah Al-Zahrah A.S with respect.

The tests described in this research were performed at the Institute of Structural Engineering, University of Kassel. I would like to express my thankfulness for my supervisor Prof. Dr.-Ing Ekkehard Fehling for his appreciated guidance, suggestions and supports during research effort.

I would like also express sincere appreciations to Dr.-Ing.Thomas Hahn head of Central Laboratory - Institute of Structural Engineering, Mr. Klaus Trost, Dip.-Ing. Beniamin Faion, as well as Mr.Burkard Deiß of the Institute of Structural Materials.

Special Thanks to Mrs. Ute Müller, and all my colleagues, Dip.-Ing.Jenny Thiemicke, Msc.Mohammed Ismail, Dr.-Ing.Torsten Leutbecher, Msc. Majed Alkhoury, Msc. Yuliarti Kusumawardaningsih, MSc. Paul Lorenz for their co-operation.

Abstract

At the Institute of Structural Engineering of the Faculty of Civil Engineering, Kassel University, series tests of slab-column connection were carried out, subjected to concentrated punching load. The effects of steel fiber content, concrete compressive strength, tension reinforcement ratio, size effect, and yield stress of tension reinforcement were studied by testing a total of six UHPC slabs and one normal strength concrete slab.

Based on experimental results; all the tested slabs failed in punching shear as a type of failure, except the UHPC slab without steel fiber which failed due to splitting of concrete cover. The post ultimate load-deformation behavior of UHPC slabs subjected to punching load shows harmonic behavior of three stages; first, drop of load-deflection curve after reaching maximum load, second, resistance of both steel fibers and tension reinforcement, and third, pure tension reinforcement resistance. The first shear crack of UHPC slabs starts to open at a load higher than that of normal strength concrete slabs. Typically, the diameter of the punching cone for UHPC slabs on the tension surface is larger than that of NSC slabs and the location of critical shear crack is far away from the face of the column. The angle of punching cone for NSC slabs is larger than that of UHPC slabs. For UHPC slabs, the critical perimeter is proposed and located at 2.5d from the face of the column. The final shape of the punching cone is completed after the tension reinforcement starts to yield and the column stub starts to penetrate through the slab.

A numerical model using Finite Element Analysis (FEA) for UHPC slabs is presented. Also some variables effect on punching shear is demonstrated by a parametric study.

A design equation for UHPC slabs under punching load is presented and shown to be applicable for a wide range of parametric variations; in the ranges between 40 mm to 300 mm in slab thickness, 0.1 % to 2.9 % in tension reinforcement ratio, 150 MPa to 250 MPa in compressive strength of concrete and 0.1 % to 2 % steel fiber content. The proposed design equation of UHPC slabs is modified to include HSC and NSC slabs without steel fiber, and it is checked with the test results from earlier researches.

Contents

Symbols and Notations

A	non dimensional constant = 0.24
B_o	critical shear perimeter for normal strength concrete
B	non dimensional constant = 16
b_o	critical shear perimeter of UHPC located at specified distance from the face of the column
b_{of}	modified critical shear perimeter taking into account the fiber content effect
C_u	creep coefficient
CFRP	carbon fiber reinforced polymers
COV	coefficient of variations
c	column dimension
d	effective depth of concrete
D	diameter of steel fiber
D_f	bond factor for NSC (0.5 for round fiber, 0.75 for crimped fibers and 1.0 for duoform fibers)
E	modulus of elasticity of concrete
f_c	compressive strength of concrete
f_y	yield stress of tension reinforcement
f_{tm}	matrix tensile strength of fiber reinforced concrete
f_{te}	fiber efficiency of tensile strength in fiber reinforced concrete
FEM	finite element method
FRP	fiber reinforced polymers

F	fiber factor
GFRP	glass fiber reinforced polymers
G1Ufib0.5	ultra high performance concrete slab with 0.5% steel fiber
G1Ufib1.1	ultra high performance concrete slab with 1.1% steel fiber
G1Ufib0	ultra high performance concrete slab without steel fiber
G2Nfc40	normal strength concrete slab with compressive strength of 40 MPa
G3Uϱ1%	ultra high performance concrete slab with 1% reinforcement ratio
G4Ut55	ultra high performance concrete slab with 55 mm thickness
G5Ufy560	ultra high performance concrete slab with normal yield strength steel bars
G	shear modulus of elasticity
h	slab thickness
H.S.S	high strength steel bar
K	the non-dimensional constant value (= 0.45)
LVDT	linear variable displacement transducers
L	length of steel fiber
M3Q	concrete mix proportion used for ultra high performance concrete
NSC	normal strength concrete
N.S.S	normal strength steel bar
SFRC	steel fiber reinforced concrete
UHPC	ultra high performance concrete
Vb	vertical fiber pull out stress along inclined crack
v	poisson's ratio

V_f fiber volume fraction

V_{exp} experimental punching load

V_{pro} proposal punching load

V_{num} numerical punching load

w/b water to binder ratio

Θ angle of punching cone

ϱ tension reinforcement ratio

ξs constant depth factor =1.4

ε_u ultimate strain of tension steel bars

Δ_d relative displacement of steel reinforcement due to dowel action

β_d size effect factor

β_ϱ reinforcement ratio factor

Chapter One

Introduction

1.1 General

Flat slabs are widely used in multi-story buildings such as office buildings and car parks. A flat slab is a reinforced concrete slab supported directly on columns without any intermediary beams; see Figure 1.1. The slab may be in the area of the column of constant thickness or it may be thickened as a drop panel. The column may also be of constant section or it may be changed to form a column head or capital. The drop panels are effective in reducing the shearing stresses where the column is liable to punch through the slab, and they also provide an increased moment of resistance where the negative moments are greatest.

The flat slab system has many advantages over the slab-beam system. The simplified formwork and the reduced story heights make it more economical. Windows can extend up to the underside of the slab, and there are no beams to obstruct the light and the air circulation. HVAC installation may place continuously underneath the slab and above the suspended ceiling.

One of the major design problems for flat slab structures lies in the large bending moments and shear force generated at the intersection between the slab and the supporting columns. The focus in this study is on the punching shear stress.

Punching shear failure is a local phenomenon which generally occurs in a brittle manner, at concentrated load or column support region. This type of failure is catastrophic because no external, visible signs are shown prior to occurrence of the failure. Punching shear failure disasters have occurred several times in the last decades. In June 30, 1995, a five story department store in South Korea collapsed due to punching shear failure. In this disaster, 500 people were killed and almost 1000 people were injured, see Figure 1.2.

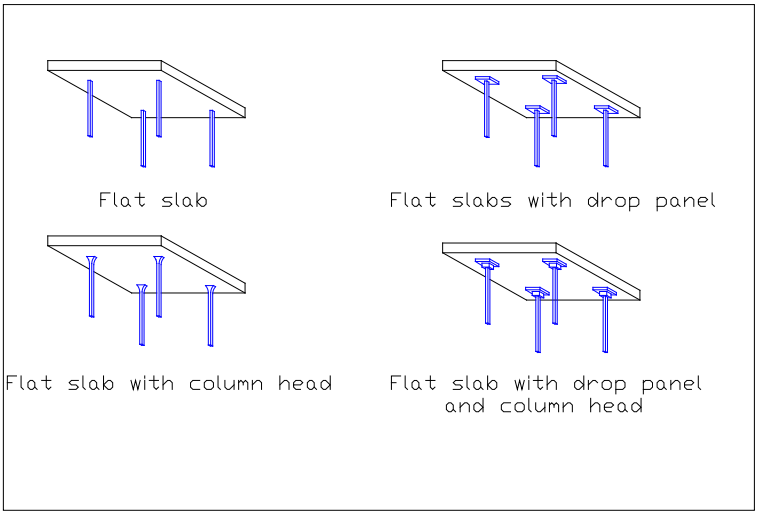

Fig. 1.1: Flat slab building

Fig. 1.2: Post-collapse photograph of the Sampoong Department Store

A typical flat slab punching shear failure is characterized by punching of a column through a portion of the surrounding slab. Figure 1.3 shows an example of a punching shear failure. This type of failure is one of the most critical considerations when determining the thickness of flat slab at the slab-column intersection. Therefore, the safe design of concrete flat slabs is of great importance and the accurate prediction of punching shear strength is a major concern for design of flat slab.

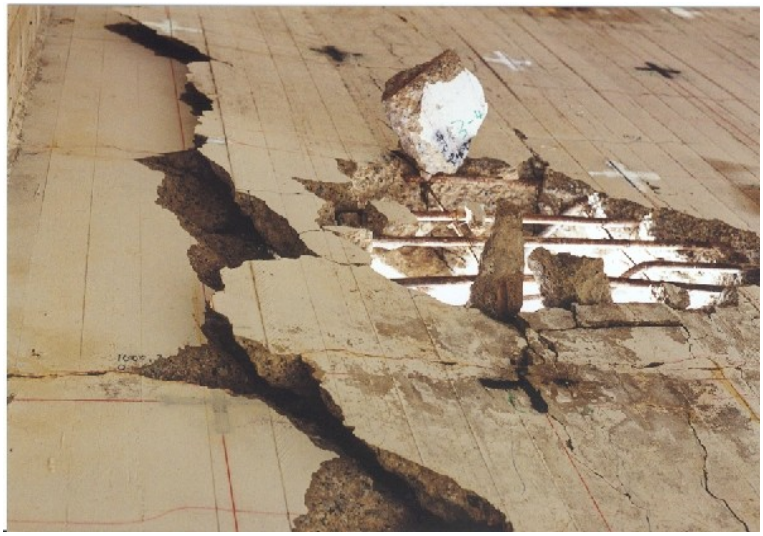

Fig. 1.3: Punching shear failure in a bridge deck [16]

1.2 Punching Shear Failure

For the slab-column connection, the punching shear strength is defined as the net ultimate reaction at the column's contraflexural points and the failure can be generally classified as either flexural or shear, depending on whether the failure is initiated by yielding of reinforcement, crushing of concrete and formed internal diagonal cracking.

When a reinforced normal strength concrete (NSC) flat slab structure is subject to heavy gravity load, punching shear cracks occur at slab tension surface in column vicinity, they propagate at 20^{o}-50^{o} angles through the slab thickness to form a truncated conical or pyramid failure surface around the column. In addition to vertical loads, the slab-column connections may be subject to unbalanced moments, which may be caused for example by unequal spans on both sides of the column or by lateral loading such as wind or earthquakes. The unbalanced moment is resisted by a combination of stresses in slab flexural reinforcements, shear strength of concrete, and shear reinforcement in the vicinity of the column.

The punching shear failure mechanism of the NSC slab under punching shear usually starts with flexural cracking in the tension area directly under the support column. These cracks are distributed in radial and tangential directions with load increasing till the critical shear cracks open and then are distributed to form the failure cone diameter at the tension area. Shear cracks move towards the compression area through the thickness of the slab to form the whole punching shear cone, see Figure 1.4.

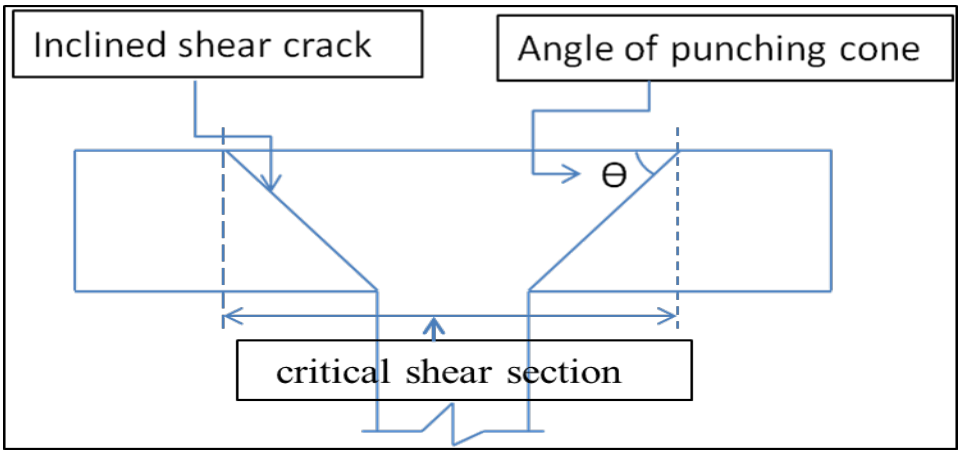

Fig. 1.4: Punching shear failure

The most important factors affecting on punching shear failure mechanism of NSC slabs are:

- **Concrete Strength:** Many researchers believed that the punching strength of NSC slabs occurs due to crushing of concrete and the shear strength is controlled by the concrete strength. Regan [48] plotted the punching load against the concrete strength and the resistance is proportional to the cubic root of the concrete compressive strength, as can be seen in Figure 1.5. The B.S 8110, DIN-1045 and CEB codes take punching strength to be proportional to the cube root of the concrete strength. The ACI code uses the square root of concrete strength to be proportional to the punching strength.

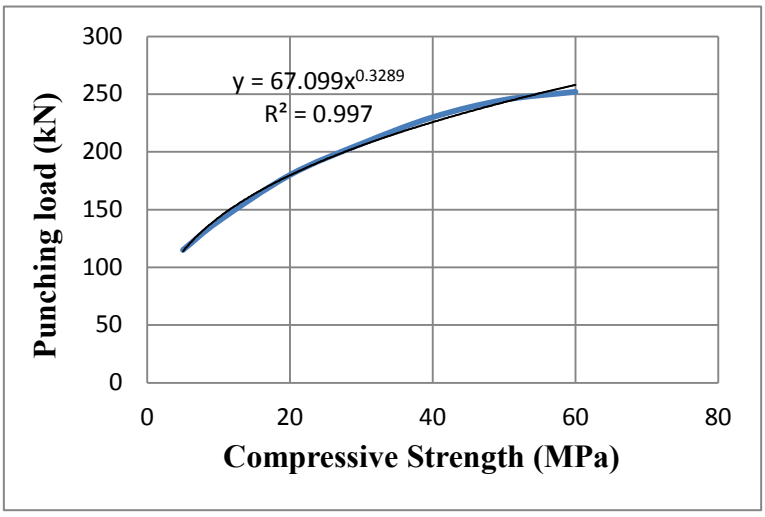

Fig. 1.5: Relation between compressive strength and punching load [48]

- **Ratio of Tension Reinforcement**: Punching shear strength is expected to increase with tension reinforcement ratio increasing due to increased depth of compression zone. This effect is included in DIN-1045-1 and B.S 8110 code of practice with power function of (1/3) but it is not included in ACI code. In the test of Regan [48] shows in Figure 1.6, the reinforcement ratio is increased from 0.83% to 1.52% and consequently the punching load increased.

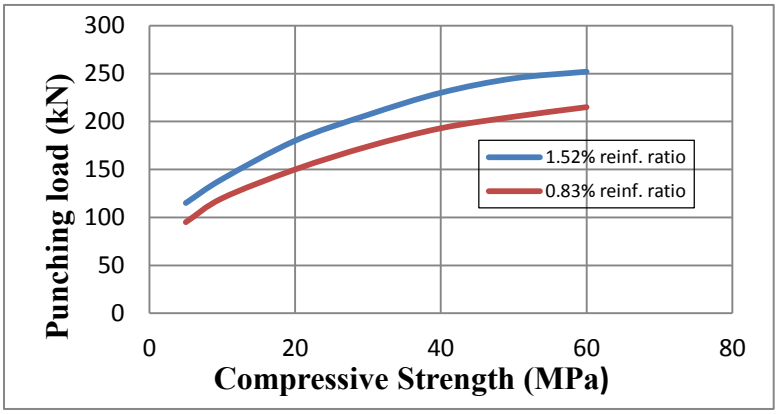

Fig. 1.6: Effect of reinforcement ratio on punching strength according to [48]

- **Size effect:** Tests results of many researches showed that the punching shear strength of slab increases with decreasing the slab thickness. Regan [48] tested six specimens and the test results show that the punching shear strength agree with the size factor of British standard $(1/d)^{1/4}$.
- **Effect of Span / depth ratio:** Lovrovich and McLean [36] tested slabs with varying span to depth ratio. They found that the punching shear strength of slabs significantly increased for span to depth ratio below six; see Figure 1.7. Span in this case means the length between the supports of the test specimen, i.e. length between lines of inflexion.

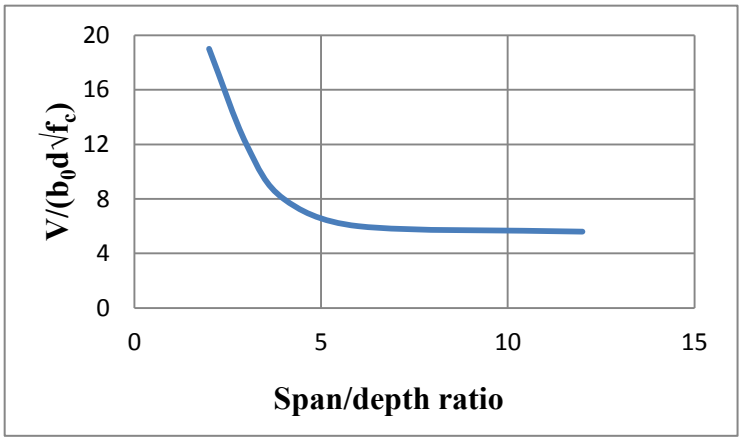

Fig.1.7: Effect of span / depth ratio according to [36]

1.3 Ultra High Performance Concrete (UHPC)

Advanced knowledge and understanding of the behavior of concrete on the micro-structural level have led to the development of the next generation of concrete, namely **Ultra High Performance Concrete (UHPC)**.

UHPC is a relatively new material in the market, relies on the same principles as conventional concrete, but provides improved mechanical properties resulting from changing in the blend composition. The compressive strength of UHPC is between 6 to 10 times of that of NSC. Additionally, UHPC with fibers exhibits a tensile strength unheard of that in conventional concrete, allowing for the possibility of eliminating traditional steel reinforcement in some applications. The use of UHPC allows for section dimensions to be minimized, taking advantage of the improved material properties while minimizing material usage and cost. In addition to the improved strength properties, UHPC maintains a very low permeability, making the material resistant to corrosion and deterioration often associated with normal reinforced concrete and steel structures. The resistance directly correlates to a longer service life that can be achieved with the use of UHPC, making it an ideal material for a number of structural applications.

The benefits of UHPC are quite substantial, but are offset by the high cost of the material. With the material being relatively new, there have only been a limited number of structural applications and the costs have remained high because the material is still considered to be a specialty product. The expectation is that as the design with UHPC becomes more common practice; the costs will decrease as the industry becomes more familiar with this material.

1.4 Project Scope

The main objectives of this study are:

- Study the modes of failure of UHPC slab-column connection under punching load through an experimental program.
- Determine the punching shear angle and critical shear perimeter of UHPC slab-column connection.
- Present a numerical model for UHPC slab-column connection under punching shear using Finite element analysis for further parametric study.
- Present design equation for the prediction of the punching shear capacity of UHPC slabs.

Chapter Two

Literature Review

2.1 Introduction

Flat slabs is a kind of structure widely used for construction of multi-story buildings, as such a significant number of research works have been published on the punching shear failure of concrete flat slabs. These will be presented herein. Additionally, the finite element method used for the analysis of punching shear failure of reinforced concrete flat slabs has also been presented.

UHPC is a relatively new type of concrete; therefore a limited amount of researches has been performed, leaving several opportunities for the characterization of the behavior, at material and structural level with rare researches specifically devoted to the punching shear capacity for the UHPC slabs.

2.2 Ultra High Performance Concrete (UHPC)

2.2.1 Definition

UHPC is the type of concrete that has superior properties in comparison with conventional concrete. The main characteristics of UHPC is a compressive strength up to 250 MPa, a higher ductility, higher tensile strength and better durability.

2.2.2 General Composition

UHPC contains some differences in the constituent materials compred to conventional concrete. Table 2.1 shows the UHPC material compositions according to M3Q mix desingn used in structural engineering department in Kassel University. For this mixture, compressive strengths reached 200 MPa.

Table 2.1: UHPC compositions

Material	Weight [kg]
water	18.3
portland cement	86.2
Silica fume	18.3
Superplasticizer	3.2
fine quarz	20.9
sand 0.125/0.5	101.9
steel fiber (0.25mm/20mm)	4.1

The most distinguishing characteristics of the composition of UHPC are the lack of coarse aggregate, use of steel fibers, high proportion of cement / cementitious material and low water to binder ratio (w/b).

UHPC is brittle material without steel fiber, so the steel fiber is added to the cement matrix to increase the ductiltly and avoide britte type of failure.

2.2.3 Mechanical Properties of UHPC

Ultra high performance concrete (UHPC) is characterized by outstanding amazing mechanical properties:

2.2.3.1 Compressive Strength (f_c)

One of the most substantial properties of UHPC is its compressive strength; UHPC has been demonstrated to achieve compressive strength (f_c) ranging from 150-250 MPa. This improvement in compressive strength has far exceeded the results achieved with NSC and may allow for the possibility of UHPC to be more competitive in markets that have been typically dominated by steel construction. Figure 2.1 shows the stress-strain relationship of a cylinder under compression for UHPC (f_c = 200 MPa) and NSC (f_c = 40 MPa), in which, the compressive strength of UHPC is 5 times of NSC. And the strain at maximum strength for UHPC is approximately 2 times that of NSC.

Interesting is, that UHPC exhibits nearly linear behavior up to 90% of its compressive strength before diverging 5 % from linear elastic behaviour (this value is 45 % for NSC).

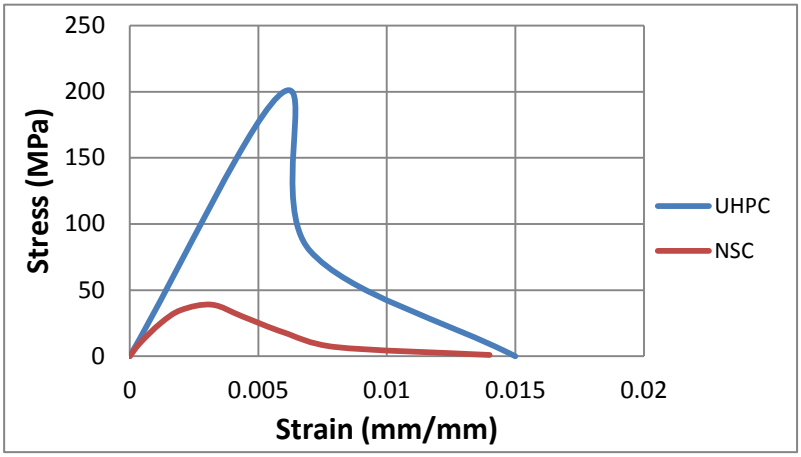

Fig. 2.1: Stress-Strain relationship in compression

2.2.3.2 Tensile Strength

The significant improvement in compressive strength is complemented by the fact that UHPC due to the effect of small high strength fibers also exhibits tensile strength that has not been demonstrated in NSC. As in NSC with steel fibers, UHPC under axial tensile force can be classified as being strain-softening or strain-hardening, depending on amount of steel fiber content. The matrix tensile stress (f_{tm}) is defined as the stress when the first percolation crack occurs. And f_{te} is defined as post cracking fiber efficiency of tensile stress. The ratio between the tensile strength of UHPC with 1.1% steel fiber and the tensile strength of NSC can be 2.8, see Figure 2.2. In the example, the fracture energy which represents the area under the stress-displacement curve of UHPC is 3.8 times that of NSC.

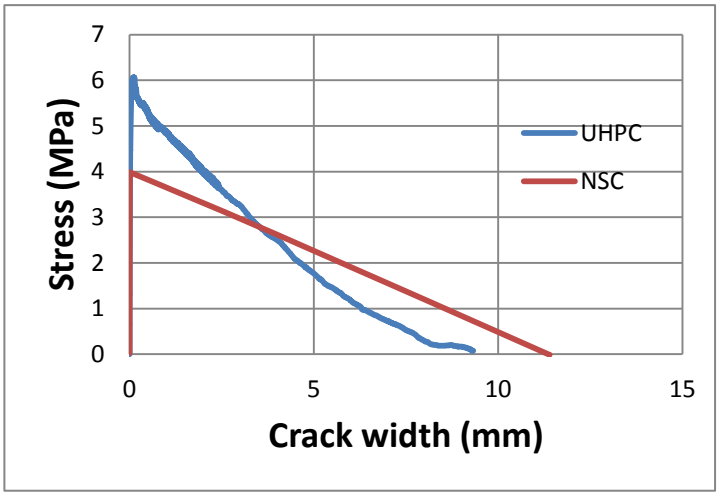

Fig. 2.2: Stress-Crack width relationship for UHPC and NSC

2.2.2.3 Other Properties of UHPC

Besides improved strength and ductility, UHPC exhibits some characteristics that make it very interesting for use in a number of applications. UHPC maintains a very low permeability-roughly $4.7x10^{-18}m^2$. UHPC allows for negligible carbonation or penetration of chlorides / sulfates and also maintains a high resistance to acid attack. UHPC has excellent resistance to freeze-thaw cycles also developed from the dense matrix, making it ideal for virtually any climate condition.

UHPC also shows very low creep and shrinkage after heat treatment when compared to NSC, making the material adequate for precast / prestress structures. The material can also be categorized as a self consolidating concrete due to the ease of flow of the material, which can be poured or pumped into place with limited or no vibration.

Design equations from the association Française de Gēnie Civil (AFGC) French Specification (2002) and Deutscher Ausschuss für Stahlbeton (DAfStb 2008) were used to estimate the modulus of elasticity for UHPC as follows:

$E = 262,000\sqrt[3]{f_c}$ (psi) .....(AFGC)

$E = 8800.f_c^{1/3}$ (SI) for fine aggregate .....(DAfStb)

$E = 10200.f_c^{1/3}$ (SI) for coarse aggregate with Basalt .....(DAfStb)

Where; f_c is the compressive strength of UHPC.

Poisson's ratio is the ratio of lateral to longitudinal strain for hardened concrete, an average value of 0.2 is justified for normal and high strength concrete, but due to the proportionally smaller lateral confinement effects, a possion's ratio of UHPC of about 0.18 can be considered [20].

The coefficient of thermal expansion of UHPC is around $15x10^{-6}$ mm/mm/C^0. This value is higher than $10x10^{-6}$ mm/mm/C^0 which normally can be expected for NSC .This is due to high cementicious component.

2.3 Advantages of UHPC

There are several advantages of UHPC when compared to NSC and even to steel in some structural applications. The high strength of UHPC allows the designer to use smaller sections, resulting in use of less material to get the same capacity. The presence of the steel fibers in UHPC allows in some cases for cancellation the flexural and shear reinforcement. Due to the high durability, UHPC structures are expected to have a longer service life than conventional concrete structures. UHPC is also able to resist the effects of severe environments and to save money in overall project life.

2.4 Disadvantages of UHPC

The biggest disadvantage of using UHPC is the initial cost. With UHPC being relatively new material to the industry, there have been only a limited number of applications. The design and use of this material has not yet been optimized or streamlined and as result, the cost is still typically higher than NSC. As UHPC becomes more common in practice, the cost of use will decrease and saving will be achieved over the life cycle when compared to conventional solutions.

2.5 Previous Research on Punching Shear of Two Way Slab

Kinnunen and Nylander (1966) [60] presented a mechanical punching model based on experimental observations on circular slabs under concentric punching loads. The model is based on truncated cones which are limited confined by the shear crack and divided by radial cracks. Each segment is assumed to act as a rigid body which is supported by an imaginary compressed conical shell placed between column and root of the shear crack (Figure 2.1c and 2.1d).

At the failure load, each rigid segment rotates about the center of rotation (CR), and different forces are acting on each segment. The ultimate punching load can be found from the equilibrium equations of the forces at each segment. Failure occurs when the concrete strain at the bottom surface of slab under the compressed conical shell reach a critical value.

At the time of failure, the tension reinforcement yields in the radius r_s at the top area of the slab. The radius r_s is measured from the center of the column. If the radius of failure r_s is larger than $l/2$, yielding occurs in the whole reinforcement

which is in the area of the radius r_s. At this point, the ultimate load is equal to the flexural failure load. If the radius of failure r_s is smaller than $l/2$, yielding occurs within r_s, and the ultimate load is less than the flexural failure load.
The punching load is calculated from Equations 2.3 and 2.4 given below. Equation 2.3 indicates that the punching shear resistance of the slab is highly dependent on the ratio of column width and effective depth of slab (c/d).

From vertical equilibrium of the segment (Figure 1.2b);

$$P = T\sin\alpha \qquad \text{.....(2.1)}$$

$$T = \sigma_{cs} A_{cs} \qquad \text{.....(2.2)}$$

$$P = \pi\left(\frac{c}{d}\right)\left(\frac{x}{d}\right)\left(\frac{c+2x}{c+x}\right)\sigma_{cs} f(\alpha) d^2 \qquad \text{.....(2.3)}$$

Taking moments about the point of intersection of $T\Delta\varphi/2\pi$ in the conical shell and the resultant of the forces, R_4 , gives

$$P = \frac{2\pi}{K_y}[C1 + \rho C2]\ fyd \qquad \text{.....(2.4)}$$

Where $$f(\alpha) = \frac{\tan\alpha(1-\tan\alpha)}{(1+\tan)^2} \qquad \text{.....(2.5)}$$

$$K_y = \frac{3(1-c)}{2(3d-x)} \qquad \text{.....(2.6)}$$

If $r_s \geq C_o$ $\qquad C_1 = (r_s - C_o) + r_s \ln(l/2r_s), \quad C_2 = C_o\Delta\varphi$

If $r_s \leq C_o$ $\qquad C1 = r_s \ln(l/2C_o), \quad C_2 = r_s\Delta\varphi$

And;

P is the punching load
T is the compressive force in conical shell
α is the angle of the compressive force in the conical shell
σ_{cs} is the stress in the conical shell
A_{cs} is the cross section area of the conical shell

c is the diameter of column
d is the effective depth of slab
f_y is the yield stress of reinforcement ratio
l is the diameter of slab
x is the neutral axis depth
C_0 is the radius of shear crack
r_s is the radius of yielded reinforcement
$\Delta\varphi$ is the angle of sector element

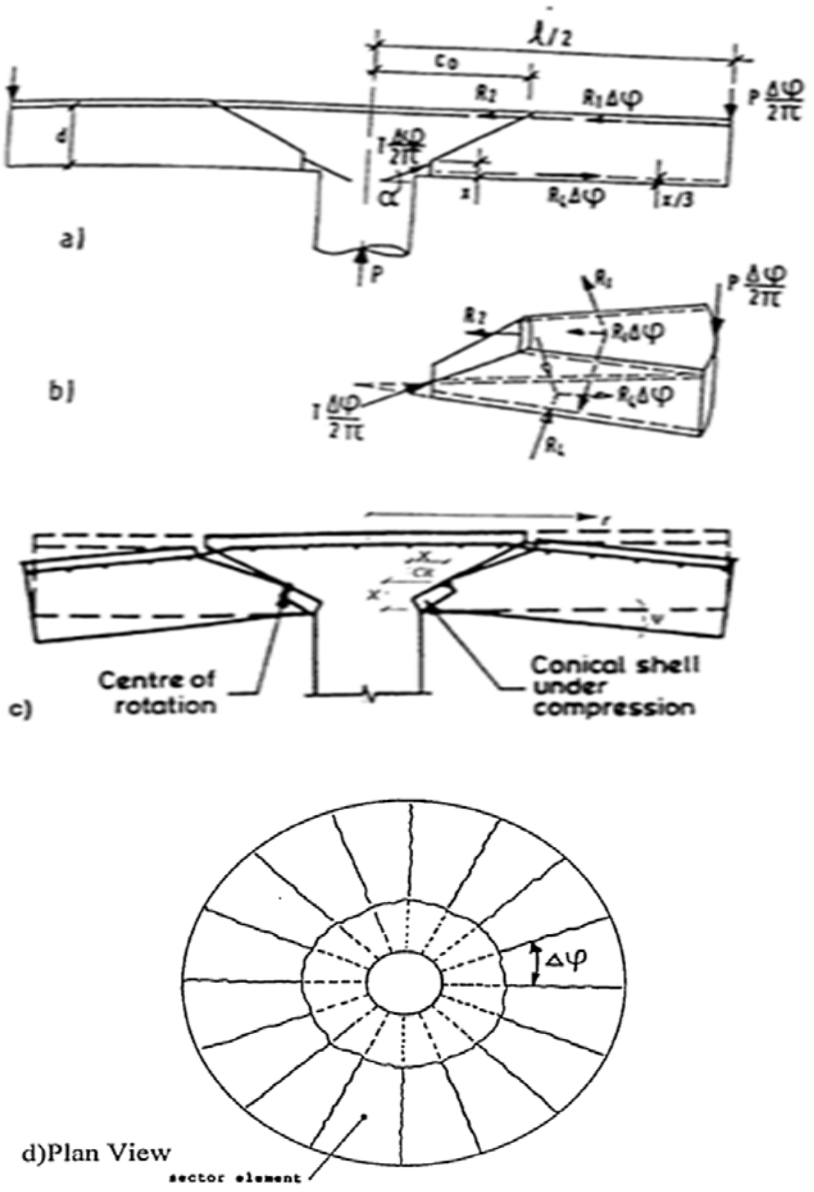

Figure 1.2: Kinnunen-Nylander punching model

Yitizhaki[(1966)] [15] presented a method for calculating the punching shear strength of two way slabs. The relation between the punching shear resistance and flexural resistance of the slabs was also presented. He determines that the punching strength depends mainly on the flexural reinforcement strength (f_y) and concrete compressive strength (f_c). The punching shear strength at distance d from the face of the column, can be calculated from:

$$V_u = (149.3 + 0.164\, \varrho f_y)\, [1-(0.5\varrho f_y) / f_c]\, b_o.d \qquad \text{.....(2.1)}$$

Where; ϱ is the tension reinforcement ratio, b_o is the critical shear perimeter at distance d from the face of the column, d is the effective depth of the slab.

Regan[(1984)] [48] investigated forty simply supported slabs with the distance between the load and support short enough for the shape of failure surface to be described by the specimen geometry. The results gained are used to derived an easy empirical expression for punching strength in terms of the geometry of the punching cone.

Regan[(1986)] [49] tested twenty eight reinforced concrete slabs taken into account the influence of the arrangement of flexural reinforcement, depth of the slab, concrete compressive strength, ratio of tension reinforcement, boundary restraint and the size of the loaded area on punching of reinforced concrete slabs. He conclude that concentration of reinforcement toward the loaded area has no meaningful important effect in terms of punching resistance; the punching resistance of the slabs can be appreciably improved when the boundary conditions are other than those of simple support.

Narayanan and Darwish[(1987)] [55] disscussed the influence of steel fiber reinforcement on the punching shear capacity of micro-concrete slabs by testing twelve simply supported slabs up to failure. The variables studied were the volume fraction of fibers, tension reinforcement ratios and concrete compressive strength. The results reported that an increase in fiber content improved the shear strength

and adjusted the position of the critical perimeter. They suggested the following equation:

$$V_u = \xi_s (A \cdot f_{ct} + B \cdot \varrho + V_b) \quad \text{.....(2.2)}$$

ξ_s = empirical depth factor =1.4
A= non dimensional constant =0.24
f_{ct} = split cylinder strength of fiber reinforced concrete, MPa
B = dimensional constant = 16
V_b= vertical fiber pull out stress along inclined crack, MPa

Gardner(1990) [47] inspected researches and code provisions on the punching shear capacity and its correlation to concrete strength. He showed results of an experimental investigation relating punching shear to concrete strength and steel ratio. He believes that shear capacity is proportional to the cube root of concrete strength and steel ratio and that ACI-CSA code provisions should be reviewed.

Broms(1990) [8] demonstrates a design method to calculate the punching strength and deflection of flat plates at interior columns. Failure is assumed to take place when the compression zone of the slab in the vicinity of the column is distressed by either a high radial compression stress or by a high tangential compression strain. Size effect and the influence of increasing concrete brittleness with increasing strength are both considered. The method appears to be in excellent agreement with results from punching tests reported in the literatures, with conditions ranging from ductile flexural failures to brittle punching failures, from small test specimens to a full sized structure, from symmetrical to unsymmetrical loadings, and from low to high concrete strengths and reinforcement ratios.

Lovrovich and McLean(1990) [36] presented results of an experimental investigation of the punching shear capacity of reinforced concrete slabs with varying span-depth ratios. Ten axisymmetric slabs were analyzed; five with flexural reinforcement and five with both flexural and shear reinforcement. The slab thickness was kept constant while the support diameter was changed to reflect different span-depth ratios. The punching shear capacity was found to substantially

increase as the span-depth ratio decrease below 6. Maximum test capacity was nearly five times greater than the 1983 ACI building code predicted capacity. The higher capacity was a result of smaller span-depth ratios, in plane compressive forces caused by restraining action at the supports, and excellent anchorage provided for the shear reinforcement.

Marzouk and Hussein[(1991)] [29] analyzed seventeen reinforced concrete slabs to check the deformation and strength characteristics of punching shear failure of high strength concrete slabs. The tested specimens had different slab depths and reinforcement ratios changing between 0.49 and 2.33 percent. Experimental results demonstrate that as the amount of reinforcement is increased, the punching strength of the slabs is also increased. It was found that using the cubic root of the concrete compressive strength to calculate the punching resistance of the concrete slabs generally give good results than the square root expression used in ACI Codes.

Alexander and Simmonds[(1992)] [59] presented an experimental program designed to compute the straight line strut and tie model for evaluating punching shear capacity. Eight isolated column flat plate connections were loaded to failure. The main variables were clear cover, spacing of reinforcement through the column, and the boundary restraint. Measurements of strain were made along reinforcement passing through and immediately adjacent to the column. These measurements do not support the concept of an inclined straight line compression strut as assumed in the strut and tie model, but demonstrate that the compression strut is more in the shape of an arch. The advantageous effect of increased cover in improving the shear capacity and connection ductility is certified. Increasing the amount of slab reinforcement passing through the column can lead to anchorage failures. An anchorage failure of this reinforcement is not distinguishable from a punching failure on the basis of external appearances during or after a test and it is believed that many punching failure reported in the literatures were limited by anchorage capacity.

Kuang and Morley[(1992)] [35] investigated twelve restrained reinforced concrete slabs. The slab panels were supported and restrained on all four sides by edge beams. The effect of the degree of edge restraint, percentage of steel reinforcement, and span-depth ratio of the slabs was determined. The punching shear strengths observed were much higher than those calculated by Johnson's yield line theory, BS 8110, and ACI 318. The improvement punching shear capacity was a result of compressive membrane action caused by restrained action at the slab boundaries.

Marzouk and Chen[(1993)] [30] presented an analytical analysis on the behavior of reinforced high strength concrete slabs. A plasticity based concrete model is used for the finite element analysis. An eight-node quadrilateral shell element with a reduced 2x2 Gaussian integration over the element plane and nine point Simpson type integration through the element thickness are applied. An acceptable post cracking tensile model of reinforced high strength concrete is applied based on the fracture energy of high strength concrete reported from stress-displacement curves (stress-crack width curve). The validity of the developed model is then approved by comparison with the test results of reinforced high-strength concrete slabs. Finally, the behavior of such slabs is checked through a parametric study. The sensitivity of the material model to different material properties and edge restrains is also reported in the parametric study.

Shaaban and Gesund[(1994)] [3] showed experimental study to investigate whether addition of steel fibers to the concrete mix could definitively increase the punching shear strength of reinforced concrete slabs. Thirteen slab specimens and their companion cylinder specimens were tested. Fiber concentrations in the slabs ranged from 0 to 6.4 percent by weight of concrete. The test demonstrate that the addition of steel fibers to the concrete mix does substantially enhance the punching shear strength of the slabs. An improvement of the ACI code design equation for shear punching strength of slabs is proposed to consider the strength increase produced by the fibers. The tests also demonstrate information on the shape and inclination of the fracture surface, and indicated that only a small, shallow region

of the slab in the vicinity of the slab column intersection is highly stressed in tension before failure.

Marzouk *et.al*(1998) [26] tested slab-column connetions under combinations of gravity and lateral load to investigate the effect of using high strength concrete slab on the structural behavior of slab-column connections. The vairables chosen for this study are the strength of concrete slab, the flexural steel reinforcement ratio, and the moment to shear ratio. As the concrete slab strength increases from 35 to 75 MPa, the shear capacity increases by 7 to 15% for loading cases of zero and high moment shear ratio respectively. The use of high strength slab has substantial effect on load deflection characteristics for specimens subjected to high moment. The ultimate deflection increases and failure mode becomes less sudden and more gradual, if high strength concrete is used. The first yielding for specimens constructed with high strength concrete slab occurs at a load essentially lower than those for specimens constructed with normal strength concrete. The radius of yielding significantly increases for specimens constructed with high strength concrete slab; therefore, the steel reinforcement is utilized better and a much more desirable steel stress distribution is produced in the area around the column by the use of high strength slab. In the meantime, connection displacement and rotation ductility, increases by 75% for specimens with high strength concrete slabs under high moment. Therefore, the use of high strength concrete slabs can be justified economically when a good ductility and higher levels of absorbed energy of slab column connections are required under high moment / shear ratios. On the other hand the use of high strength concrete slabs for slab-column connection subjected to gravity loads only is not recommended due to the small increase of the punching shear capacity of the connection compared to the high cost of using high strength concrete.

Menétery(1998) [51] showed expermintally flexural and punching failure tests on flat slabs by governing the vertical displacement under the column. This allows the monitoring of the descending branch of the load displacement curve, and demonstrates that flexural failure is characterized by a smooth decrease of the load carrying capacity, whereas punching failure exhibits a sudden reduction of this

capacity. He showed that the punching load was reached for a punching crack inclination of about 30 degree to middle plane of the slab. By increasing this inclination, the flexural failure load was closed and the sudden decrease of the load carrying capacity was reduced. A smooth transition between punching and flexural failure, which is governed by the punching crack inclination, is revealed and an interaction formula is proposed.

Gomes and Regan$^{(1999)}$ [54] analyzed twelve 3.0 x 3.0 x 0.2 m flat plate slabs with 200 mm square column, to examine the effect of shear reinforcement on punching resistance; for this aim, short lengths of steel I-beam were used. The shear reinforcement was arranged in circumferential layers around the columns. The most powerful practical measurement from the experimental analysis is that, the punching failure load of a reinforced concrete flat slab may at least be double with the use of suitable shear reinforcement.

Osman *et.al*$^{(2000)}$ [42] analyzed six high strength light weight slabs under concentrated loads. Four slabs were constructed of high strength lightweight concrete of compressive strength higher than 70 MPa, with the steel ratio ranging from 0.5 to 2.0 %. the two references specimens were constructed with normal strength concrete and light weight aggregates and had steel reinforcement ratios of 1 and 0.5 %. The results included the ultimate loads, deflections, modes of failure, crack patterns, ductility, concrete strain, and steel strains. The analysis results were compared with other test data on high strength and normal strength normal weight concrete slabs and code predictions for slab strength. Generally, a reduction factor of 0.85 is advised for lightweight aggregates by the ACI code. A similar reduction of 0.8 is suggested by the BS 8110 code. These reduction factors are conservative when used for high strength concrete. A reduction factor of 0.95 is more acceptable for high strength lightweight concrete, and of 0.85 for normal strength lightweight. The results briefed that the change of reinforcement has a more serious effect on general behavior of high strength lightweight concrete slabs compared with normal strength and high strength concrete slabs.

McHarg *et.al*(2000) [50] They tested six two way slab-column specimens, the parameters investigated were the placement of steel fiber reinforced concrete (SFRC) in the slab, and the concentration of slab reinforcement around the column. The influence of these parameters on the punching shear capacity, negative moment cracking, and the stiffness of the two way slab specimens were checked. The advantageous effects of concentrating the slab reinforcement near the column and of using fiber reinforced concrete are reported.

Oliveria *et.al*(2000) [16] presented a new form of inclined stirrups that is easy to make and to install, comparison tests of slabs without shear reinforcement and slabs with vertical stirrups are also reported. The inclined stirrups are shown to act well and produce punching resistance excellent to those obtained with vertical stirrups. Comparisons are made between the experimental results and calculations based on both ACI 318 95 and CEB FIP model code MC90.

Sherif and Dilger(2000) [2] presented test setup of two full 5m continuous reinforced concrete flat slabs. The first slab was tested three times to failure after it had been repaired twice. Shear failure happened at the edge and interior slab-column connections. Some slab-column connections contained shear studs as shear reinforcement. The experimental program as well as the test results related to the analyses of flat slabs and shear strength of slab column connections were presented and discussed. Based on test results, the shear strength of slab column connections in a real slab system with realistic boundary conditions was concluded. The results are compared with the provisions of ACI, and with the proposed shear strength equation. With respect to the analysis of the flat slab, the test results are compared with moments predicted by equivalent frame method (EFM) and linear elastic finite element analysis (FEM).

Nago(2001) [17] compared a total of twenty nine test results from four researches, with the values of punching strength calculated by using AS3600 (Standard Association of Australia 1994). The tests were applied on square or circular slabs supported by column stubs or loading plates, with the variety of concrete strength, slab reinforcement and slab depth. It is shown that the provisions

in AS3600 are applicable up to 100 Mpa; however, the ratios between observed and calculated loads show that AS3600 is less conservative for high strength slab.

Marzouk *et.al*(2002) [27] applied fictitious crack model and equilibrium equations to create a numerical model in order to calculate the punching load and the deformations of reinforced concrete slabs. Concrete strength, aggregate type, reinforcement ratio as well as the fracture strength properties were taken into account in creating the new model. In spite of the low tensile strength of concrete, it has considerable fracture energy, therefore the fracture process zone in front of a growing crack can contribute to the flexural concrete strength. The proposed model accounted the fictitious crack model principles. The three equilibrium equations were used on a radial segment of the slab and the influence of crack size and size effect were incorporated in the formulation. The model results were compared with the experimental results and currently available shear design formula to analyze the influence of the fracture properties on the calculated punching load. The model provide consistent and improved results compared to existing codes.

Oliveira *et.al*(2004) [18] analyzed fifteen high strength concrete slabs with rectangular supports and three different load patterns. The results appear that ACI 318-02 code previsions can overestimate punching resistance in some cases. An analysis, made using the finite element method, displays the effect of the shape of support and the pattern of loading on the distribution of shear. parameters are chosen to allow for these effects while using the control perimeter and basic shear resistance of the CEB model code 90, and it is certified that this approach provides strength estimates favorable than those of MC 90, BS 8110 and ACI 318.

Teng *et.al*(2004) [58] concentrated on the punching shear strength of slabs with openings and supported on rectangular columns. They tested twenty slab specimens under concentrated loads and they discovered that the stresses in the slabs were concentrated mostly around the shorter sides of the rectangular columns. Openings reduced punching strength considerably and, if the use of an opening is unavoidable, the best place for the opening is along the longer side of

the column. An equation for evaluating the punching strength of the slabs is proposed based on the ACI 318-02 approach. The effect of shear stress formula also takes into account column rectangularity. The efficiency of the proposed equation together with the ACI 318-02 equations has been checked with 223 data from literatures as well as with the 20 slab tested specimens.

Papanikolaou *et.al*(2005) [39] showed results from an extensive testing programme including a total of 30 reinforced concrete slabs with and without shear reinforcement, subjected to concentrated load in the middle. Shear reinforcement consists of either bent up bars or closed stirrups. calculated punching shear strengths were compared with strengths predicted from two major design codes (ACI 318 and Eurocode 2), as well as from two models from the literatures, the plasticity model and multi parameter empirical model. It was discovered that predictions by both codes were conservative in the case of slabs without shear reinforcement; Eurocode 2 and ACI 318 predictions are generally similar in this case. Less conservative predictions were found in the case of slabs with shear reinforcement, particularly in the case of Eurocode 2 that overestimated measured strengths of the slabs with stirrups. The plasticity model tended to overestimate punching strength, whereas the multi parameter empirical model allowed the best overall calculations. Finally, bent up bars appeared to be more efficient than stirrups in increasing the punching shear strength.

Baris and Bayrak(2005) [4] presented results of an experimental program on punching shear strengthening of reinforced concrete slab-column connections using carbon fiber reinforcement polymers (CFRPS). Externally fixed CFRP stirrups considered as shear reinforcement were used as a strengthening technique. The advantageousness of different patterns, detailing and various amounts of CFRP for strengthening were analyzed. It was found that the proposed method resulted in punching shear capacity increases up to 60% with respect to the specimen without any strengthening. In addition, displacement ductility and post punching resistance of the strengthened specimens increased, resulting in a more ductile failure mode than that of the references specimen. A design method based

on ACI 318-08 equations is also displayed for this innovative use of CFRP for strengthening slab column connections.

Chen and Yan Li[(2005)] [10] studies the punching shear strength and failure behavior of reinforced concrete slabs strengthened with glass fiber reinforced polymer (GFRP) laminates. The parameters of the 18 specimens studied are concrete compressive strength, steel reinforcement ratio, and the number of GFRP laminates layers. The specimens were tested simply supported along the four sides of the slabs and loaded through the stub column. The behavior of the concrete slabs reinforced with GFRP laminates in addition to steel reinforcement is compared to that of slabs with steel reinforcement. Experimental test results demonstrate that applying GFRP laminates markedly increases the punching shear capacity of slab column connections. Based on these, a design procedure is presented to calculate the ultimate punching shear strength of slab column connections strengthened by the GFRP laminates.

Muttoni[(2008)] [1] presented a mechanical analysis of the phenomenon of punching shear in slabs without transverse reinforcement on the basis of a critical shear crack theory. It leads to the formulation of a new failure criterion for punching shear based on the rotation of the slab. In the crack, this criterion describes punching shear failures determined in experimental testing well even in slabs with low reinforcement ratios. Its application needs the knowledge of the load-rotation relationship of the slab, for which a simple mechanical model is proposed. The new approach is shown to give better results than current design codes, with a very low coefficient of variation (COV). Adding for the proposed failure criterion and load-rotation relationship of the slab, the punching shear strength of a flat slab is shown to depend on the span of the slab, rather than on its thickness as often proposed.

Tian *et.al*[(2008)] [64] collected the test data for slab-column connections subjected to concentric gravity load and combined gravity and lateral loads. The strength of slab-column connection was calculated using ACI design equation. Also, they developed equations for slab-column connection subjected to gravity

load as a function of concrete strength, slab reinforcement ratio and yield strength, and the ratio of column size to slab effective depth. Also, they proposed model for strength of the connections subjected to lateral load using a beam analogy concept.

Tian *et.al*(2008) [65] presented experimental results of five large scale isolated slab-column connections subjected to three types of loading histories. The subassemblies represented typical flat plate construction designed prior to the 1980s that had low slab reinforcement ratios and discontinuous bottom reinforcement at the column. The specimens failed in punching shear after extensive slab flexural yielding under different loading conditions. The damage caused by simulated seismic loading did not minimize the connection punching capacity under gravity loading. The post-earthquake connection stiffness was significantly reduced. The flexural reinforcement ratio had a significant influence on connection strength and stiffness.

Birkle and Dilger(2008) [24] examined the effect of slab thickness on punching shear strength of flat slabs clearly prove the significant effect of size on the shear stress resistance, particularly for tests without shear reinforcement. New tests in which the slab thickness changed between 160 and 300 mm and tests by others with slabs up to 500 mm thick demonstrate that slabs without shear reinforcement thicker than approximately 260 mm may not have a high factor of safety if designed according ACI 318 05. For thick slabs with shear reinforcement, the shear stress resistance provide by concrete is also reduced but to a small amount.

Lee e*t.al*(2009) [37] determined the effect of the type of reinforcement (glass fiber reinforced polymer GFRP versus steel bar) on the punching shear resistance. In addition, the influence of concentrating the reinforcement in the immediate column region and the effect of using steel fiber reinforced concrete in the slab were also examined. The punching shear capacity, stiffness, ductility, strain distribution, and crack control were investigated. Concentration the slab reinforcement and the use of SFRC in the slab improved the punching behavior of the slab reinforced with GFRP bars. Calculations using different design guidelines

are compared to the experimental results obtained from the fiber reinforced polymer (FRP) reinforced slabs tested in their study and those tested by other researches. Concentrating the top mat of flexural reinforcement was results in better effects on punching shear strength, post cracking stiffness, and crack control.

Widianto *et.al*(2009) [61] analyzes lightly reinforced slab-column connections. Big flexural yielding is likely to occur before the calculated punching shear capacity is reached. The basic ACI 318 two way shear strength provision has not changed since 1963 and was developed based on a statistical analysis of test results on scaled specimens that were believed to have failed in shear. Several researchers appeared that the use of the basic ACI two way shear strength provision shows results that were unconservative compared with the two way shear strength of slabs in experimental tests. This paper demonstrates that the applicability of ACI 318 provisions for typical lightly reinforced slabs is questionable.

Cho(2009) [66] presented a new technique to enhance the punching shear resistance capacity in new flat plate structures using the studs with perforated steel plate reinforced at column-slab connections. Tests were take place on slabs of 3/4 scale, which were designed to fail as a result of punching shear. The slabs variables were as follows: first, stud rail as a control specimens; second, used four stud specimens with perforated steel plates with different lengths; third, used a perforated steel plate with the same length as the stud with steel plate. From the test results, the following conclusions were found: (a) the maximum strength of slabs have been designed to resist punching shear based on ACI 421 and Eurocode 2-04, and shear reinforcement for slabs has been compared with the results from the structural experimental; (b) the studs contributed substantially to the increase of ultimate strength; (c) the studs with steel plates contributed to the increase of ultimate strength.

Faria *et.al*(2011) [19] present parametric analysis regarding geometrical and material parameters affecting punching shear of flat slab with orthogonal mesh and square columns. To do this, they used 3D finite element analysis using ATENA program. It found that the compressive strength, fracture energy and reinforcement

ratio are the most effective parameters on punching shear strength. They believed that the tensile strength and modulus of elasticity do not effect the punching load, they are only important regarding punching behavior in terms of cracking and stiffness.

Higashiyama *et.al*(2011) [32] present a design equation for the punching shear capacity of steel fiber reinforced concrete (SFRC) slabs based on Japan Society of Civil Engineering (JSCE) standard specifications. They tested twelve SFRC slabs using hoocked-endes steel fibers with varying fiber dosage, slab thickness, steel reinforcement ratio, and compressive strength. The proposed design equation accounted for fiber pull-out strength and the critical shear perimeter changed by the fiber factor. Furthermore, the design equation is verified by the test data conducted by earlier researches, and consequently the design equation can predict the punching shear capacity of SFRC slabs with an applicable accuracy.

L.Moreillon, J.Naseir and R.Suter(2012) [41] presented an experimental program on thin UHPC slabs with and without conventional steel reinforcement. The goal from tests are to analyze the interaction between the thickness, the reinforcement ratio and fiber volumne on serviceablility limit state and ultimate limit state. The tests have highlighted the good contribution of UHPC combined with steel reinforcement on flexural and shear capacity. They also found that increasing in fiber content tends to decrease the strain capacity at ultimate load by locating the plastic strains of the rebars on a single macro-crack.

Comment: Based on the previous literatures review, the main type of concrete used in slabs was NSC and in several cases HSC with maximum compressive strength of 100 Mpa. There is a limited number of researches used UHPC, so it is of great interest to investigate how the UHPC can enhance the punching shear behavior of slabs with 200 MPa compressive strength.

Chapter Three

Experimental Program

3.1 Introduction

Flat slabs exhibit high stresses at the slab-column connection and most likely fail due to punching shear rather than in bending especially when a high reinforcement ratio is used. Punching shear failure is characterized by the cone type cracking and subsequent crushing of concrete in the column periphery before the steel reinforcement reaches the yield strain. This type of failure is not desired for structural engineering systems due to its brittle character. In this study, the behavior of UHPC slabs under punching load was investigated through experimental work. The focus of this investigation is on the interior slab-column connection.

3.2 Experimental Program

The experimental work was conducted in the Structural and Materials Laboratories - Institute of Structural Engineering at the University of Kassel. The experimental program can be described as follows:

A total of seven slabs were investigated: six UHPC slabs and one NSC slab. The influence of steel fiber content on the shear strength was studied on three slabs (G1Ufib0, G1Ufib0.5 and G1Ufib1.1). The concrete compressive strength was studied on two slabs (G1Ufib0 and G2Nfc40). The effect of tension reinforcement ratio was studied on two slabs (G1Ufib0.5 and G3Uϱ1%). The size effect was investigated by comparison of two slabs (G1Ufib0.5 and G4Ut55), and finally the influence of the yield stress of tension reinforcement was studied on two slabs (G1Ufib0.5 and G5Ufy560). The characteristics of the tested slabs with reinforcement details are summarized in Table 3.1.

Table 3.1: Details of tested slabs

Slab	Concrete type	f_c (MPa)	f_{tm} (MPa)	f_{te} (MPa)	h (mm)	fiber content %	E (MPa)	d_{bar} (mm)	ϱ (%)	f_y (MPa)
G1Ufib0	UHPC	198.5	4.2	-	100	0	49024	10.5	2	1320
G1Ufib0.5	UHPC	198.9	5.9	3.9	100	0.5	51810	10.5	2	1320
G1Ufib1.1	UHPC	208.2	7.1	7.9	100	1.1	52443	10.5	2	1320
G2Nfc40	NSC	40.3	2.8	-	100	0	27537	10	2	562
G3Uϱ1%	UHPC	198.9	5.9	3.9	100	0.5	51720	10.5	1	1320
G4Ut55	UHPC	199.2	6.0	3.95	55	0.5	51633	8	2	1570
G5Ufy560	UHPC	198.2	5.8	3.85	100	0.5	51521	10	2	562

In Table 3.1, the first column represents the names of the tested slabs, f_c means compressive strength of concrete, f_{tm} is the matrix tensile strength of concrete,

f_{te} is the fiber efficiency of the fiber concrete as a second tensile strength value in the post cracking range, h is the thickness of the tested slabs, d_{bar} is the diameter of reinforcement bars, ϱ is the reinforcement ratio, and f_y is the yield stress of tension reinforcement.

3.3 Geometry of Tested Slabs

All tested slabs had an octagonal shape with 550 mm long sides. The stub column has a cross section of 100 x 100 mm and a height of 100 mm. The slabs were simply supported along four edges. A specimen with these dimensions represents a model scale of about 50% to the negative bending moment region around the interior supporting column of a flat floor slab with 5 m span in both directions. The points of contraflexure are assumed to be 0.211 times the span apart from the supports. Figure 3.1 represents the prototype of flat slab structure and selected specimen. By removing the corners of the slab, the final shape of tested slabs will be according to Figure 3.2. The details of tension reinforcement used in constructing the specimens are according to Table 3.1. The service gravity load on this slab included 4.6 kN/m^2 self-weight, 1 kN/m^2 additional dead load regarding on floor finishing and partitioning walls, and 3.5 kN/m^2 superimposed live load.

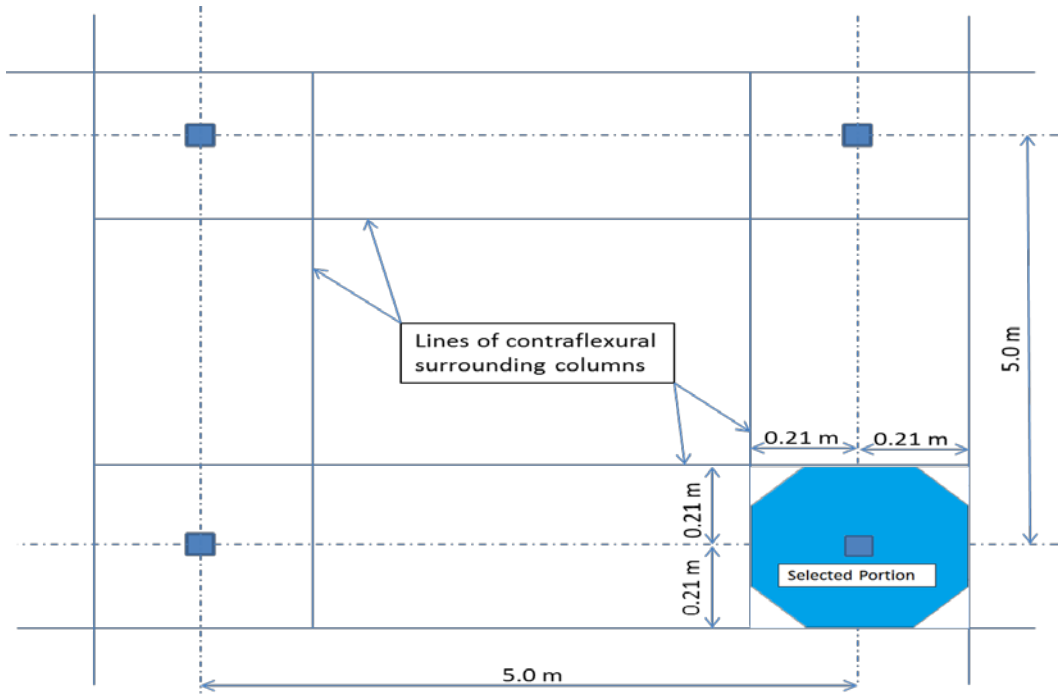

Fig. 3.1: Prototype of flat slab structure and selected specimen

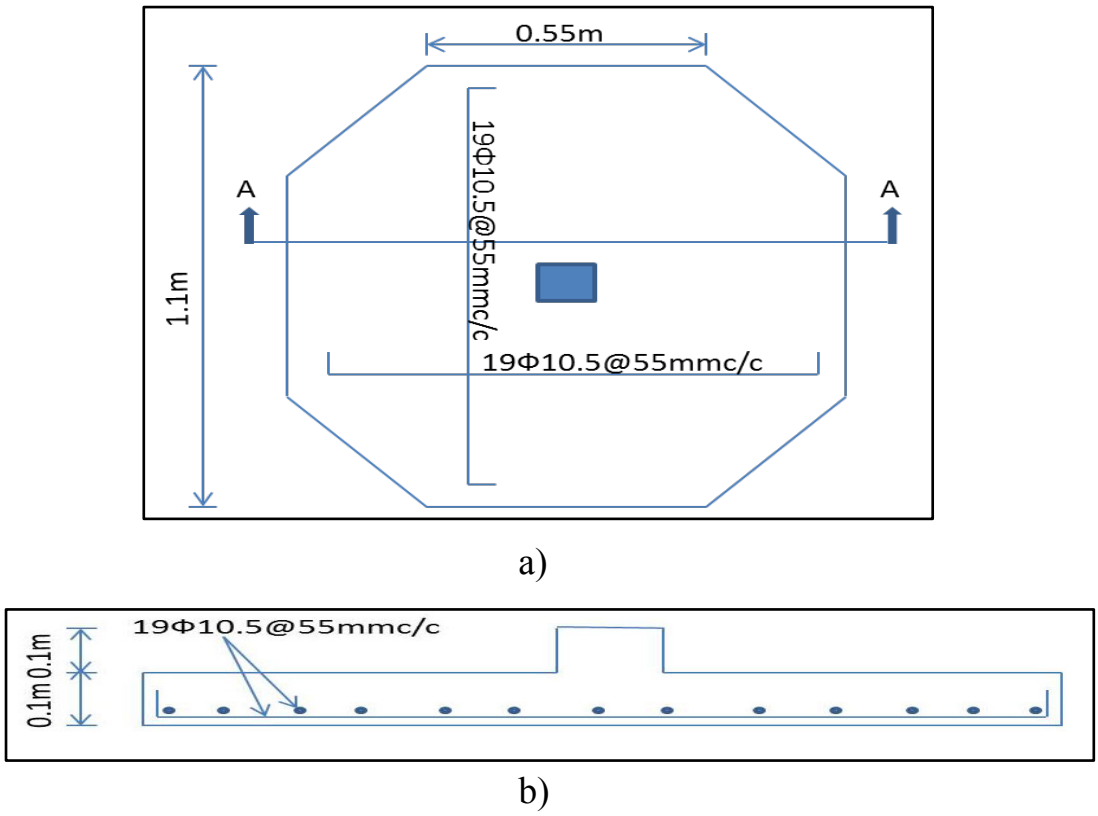

Fig. 3.2: a) Slab specimen; b) Section A-A in tested slab

3.4 Steel Fibers

Figure 3.3 shows the steel fiber type that was used in this study. This fiber has a length of 20 mm, diameter of 0.25 mm, aspect ratio of 80 and the ultimate tensile strength of 2000 MPa.

Fig. 3.3: Steel fiber used in constructing the specimens

3.5 Mix Proportion

The M3Q mix proportion was used which developed in the University of Kassel for UHPC. The appendix summarizes the compositions of the M3Q mix design for UHPC slabs and also the mix design for normal strength concrete.

3.6 Mixing Procedure

The mix procedure for UHPC slabs was made according to Table 3.2.

Table 3.2: Mix procedure of UHPC

Activity	Accumulative Time (minutes)
Dry mixing	0 - 2
Add plasticizer and water with continued mixing (3 min)	2 - 5
Break (2 min)	5 - 7
Again mixing (8 min)	7 – 15
Added steel fiber	13
Stand up	15 - 25
Pouring the concrete to the specimen	25

3.7 Concrete Properties

Two main types of concrete were used in the tested specimens: UHPC and NSC. For each type, a standard cylinder, 100 mm in diameter and 200 mm long was used to determine the compressive strength (f_c) and the modulus of elasticity (E); see Figure 3.4. The direct tensile test for notch (5mm) prisms 160 x 40 x 40 mm was used to determine the matrix tensile strength (f_{tm}), post cracking fiber efficiency of tensile strength (f_{te}) and the softening law for the tensile test; see Figure 3.5. These tests were conducted for each fiber content 0%, 0.5% and 1.1%. At least three tests in compression and nine tests in tension for each slab specimen were conducted in order to obtain the mean value of these material properties (see Table 3.1).

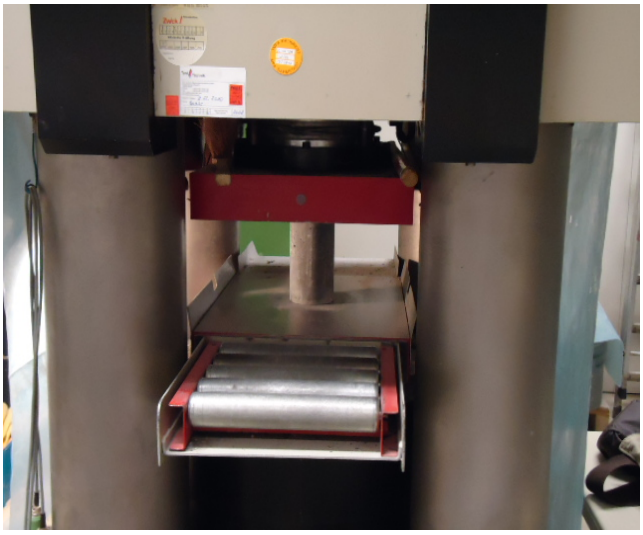

Fig. 3.4: Cylinder compression test

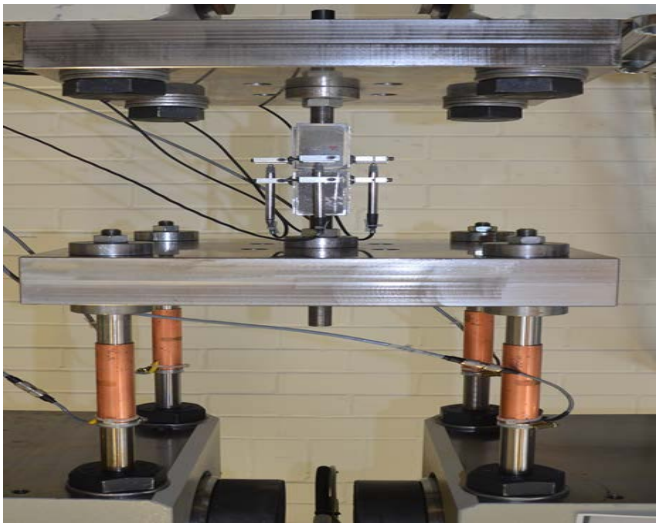

Fig. 3.5: Direct tensile test for notch prism

The compressive strength, tensile strength and modulus of elasticity of UHPC with 1.1% steel fiber were 5.16, 2.5 and 1.9 times NSC, respectively.

According to the Table 3.1, the tensile strength of UHPC with 1.1 % fiber content is 1.8 of UHPC without fibers. The ratios between the post cracking fiber efficiency and matrix tensile strength were 1.11 and 0.65 for 1.1 % and 0.5 % fiber content, respectively.

3.8 Mold and Standing Frame

The mold used for casting the octagonal slab specimens consisted of smooth 20 mm thickness coated plywood. The clear dimensions of the mold in X-Y direction were 1100 x 1100 x 100 mm. Plywood was also used for the formwork of the square column; see Figure 3.6.

The supporting frame consists of four pieces of normal strength concrete (150 x 550 x 1000) mm connected together with four pieces of U120 x 55 channels welded together. The actual shape and details of the supporting frame are shown in Figure 3.7.

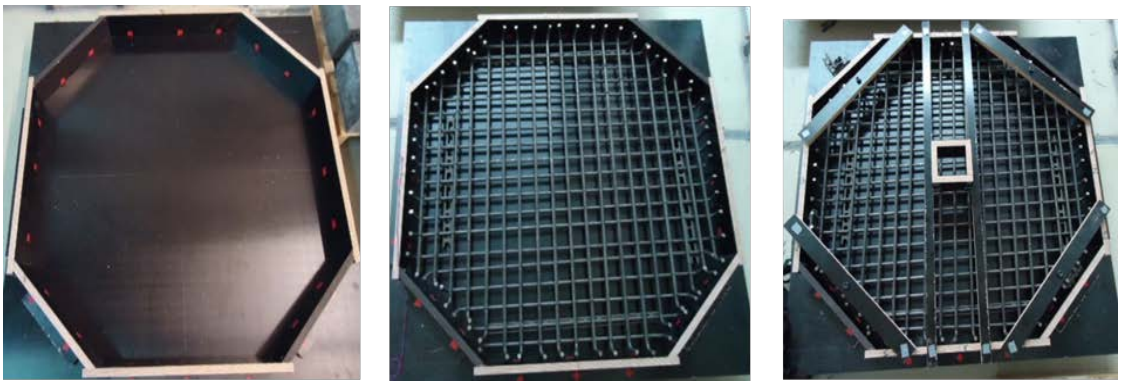

Fig. 3.6: Typical mold with reinforcement

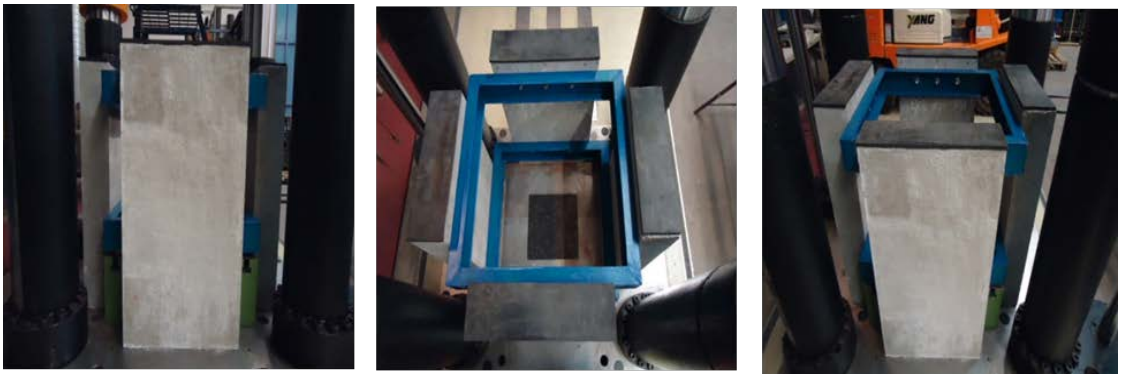

Fig. 3.7: Supporting frame

3.9 Test Setup

The tests were carried out using the hydraulic jacks of 6,300 kN in the laboratory of the Structural Engineering Institute at Kassel University (see Figure 3.8). The slabs were simply supported with edges free to rise. Rubber plates were provided under the slab where necessary to ensure uniform contact along the supports and to avoid the concrete edges splitting.

The top surface of the column stub for all slabs was filled with EuroGrout 01 material one day before testing to make the column's surface flat and to avoid non-uniform stress distribution.
The slabs were tested in an inverted position. Two cameras were used for all tests, the first at the top side (compression area) near the column and the second at the bottom side (tension area), to monitor the development of pattern cracks. Both cameras took one photo every 20 seconds.

Fig. 3.8: Testing machine and hydraulic jacks

3.10 Measurements

The applied load was measured using an accurately calibrated load cell. The vertical displacement of the specimens were measured at 12 points as shown in Figure 3.9 using linear variable displacement transducers (LVDT). The LVDTs from 1 to 4 were used to measure the vertical displacement at the center of the slabs. The LVDTs from 5 to 8 were used to calculate the deflection at 100 mm from the face of the column and from 9 to 12 to indicate the uplift vertical displacement at the edges of the slabs.

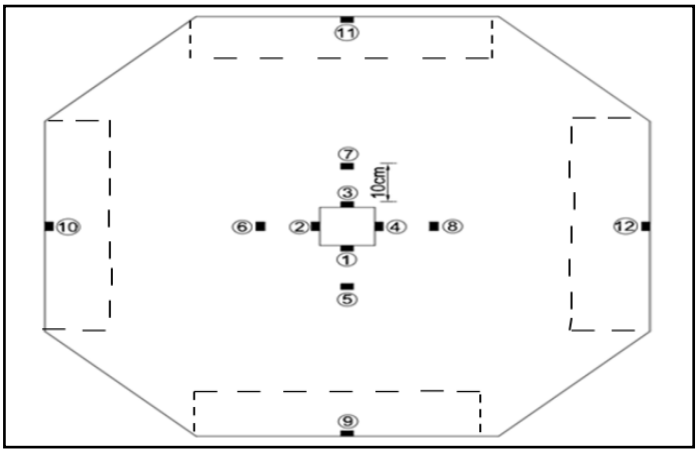

Fig. 3.9: Locations of LVTDs

3.11 Curing Process

The setting of UHPC was relatively delayed compared with conventional concrete; therefore the specimens were removed from the mold after 48 hours. Then the slab was placed in the water tank with an average temperature of 25 °C for 28 days. After that, the specimens were laid in the laboratory temperature until the date of testing.

3.12 Testing Procedure

Before testing, the supports, applied load and LVTDs were adjusted and checked; see Figures 3.10 and 3.11. The vertical load was applied to the column by displacement control of 0.01 mm/sec.

In all tests, loading was continued beyond the peak load to obtain the descending part of the load-deflection curve and to clearly see the whole punching shear cone. Cylinder compressive tests and prism tension tests were carried out approximately on the same day as the corresponding slab test. As the punching cone was completed, the load was removed to allow more photographs of the final cracks and failure patterns to be taken. The time spent in testing one specimen was about 55 to 75 minutes.

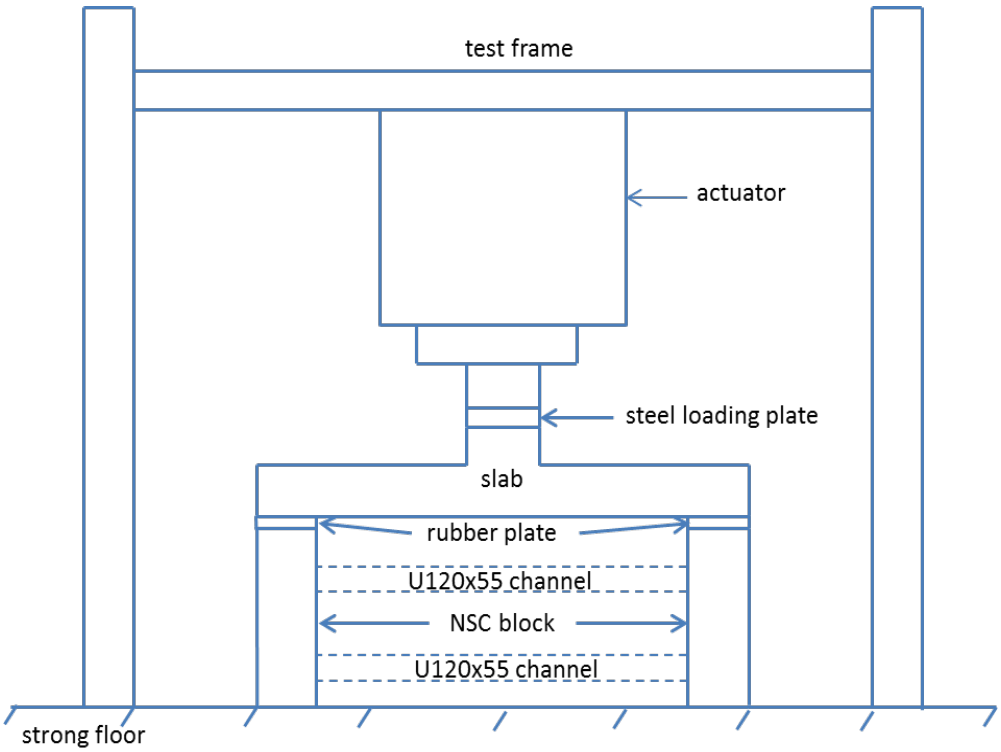

Fig. 3.10: Test arrangement

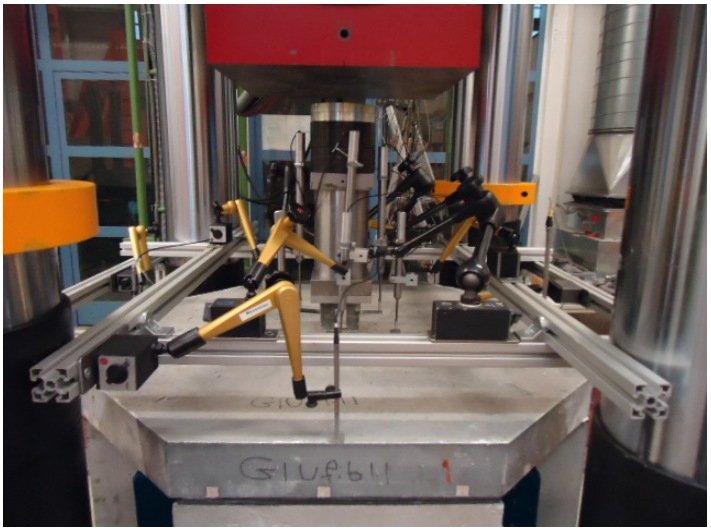

Fig. 3.11: Slab under test

Chapter Four

Test Results

4.1 Introduction

This chapter presents test results of: load-deformation behavior, first flexural crack load, opening of critical shear crack, modes of failure, flexural behavior of tested slabs at the time of critical shear crack opening, location of critical shear crack and angle of punching cone, critical shear perimeter and final shape of punching cone.

4.2 Load-Deformation Behavior

The load-deflection curves as calculated from the measured data are shown in Figure 4.1 for all tested specimens.

Figure 4.1 indicates that the type of failure is caused mainly by brittle cracking and not by a plastic mechanism. However, after reaching the peak load a residual load bearing capacity can be observed which differs in magnitude between the different test specimens.

The load and deflection characteristics can be seen in detail in Table 4.1. For all tested slabs, the load-deflection behavior in the ascending branch can be characterized by three load stages, namely first crack load, service load, and ultimate load.

The ultimate punching load ranges from 123.98 kN for the UHPC slab with 55 mm thickness (G4Ut55) to 384.5 kN for the UHPC slab with 1.1% fiber content (G1Ufib1.1). The deflection at maximum load has a band width ranging from 4.9 mm for slab G1Ufib0 to 29.68 mm for slab G4Ut55.

The post-ultimate load behavior is a very important part of the load-deflection curve of UHPC slabs as there is a big difference to post-ultimate load behavior of NSC. As illustrated in Figure 4.2, the load- bearing behavior has three stages:

First, the drop within the load-deflection curve after reaching the peak load for all slabs except the UHPC slab with 55 mm thickness (G4Ut55). This slender slab shows only a gradual drop of the load-deflection curve which means that this slab exhibits dominant flexural behavior before the punching shear failure.

Second, after the drop in the load-deflection curve, the resistance mechanism due to the fibers and reinforcement starts. Since slabs G2Nfc40 and G1Ufib0 did not have fibers, there is only reinforcement resistance.

Third, after finishing the stage of fibers and reinforcement bars resistance, the stage of pure reinforcement bars resistance to applied load according to membrane action starts. This stage starts early for slabs G2Nfc40 and G1Ufib0 due to the absence of steel fibers.

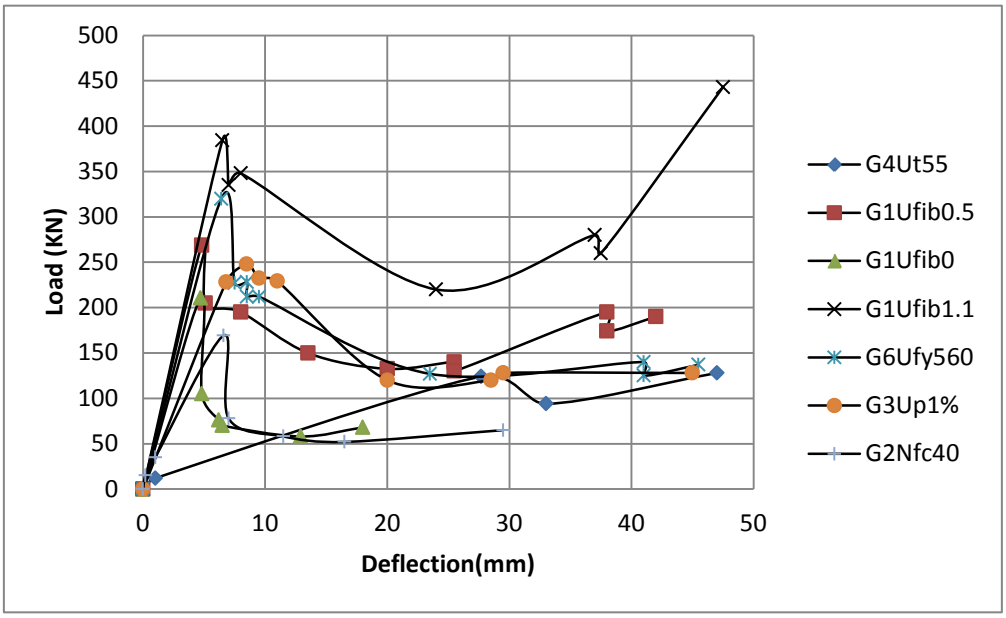

Fig. 4.1: Load-deflection curve of tested slabs

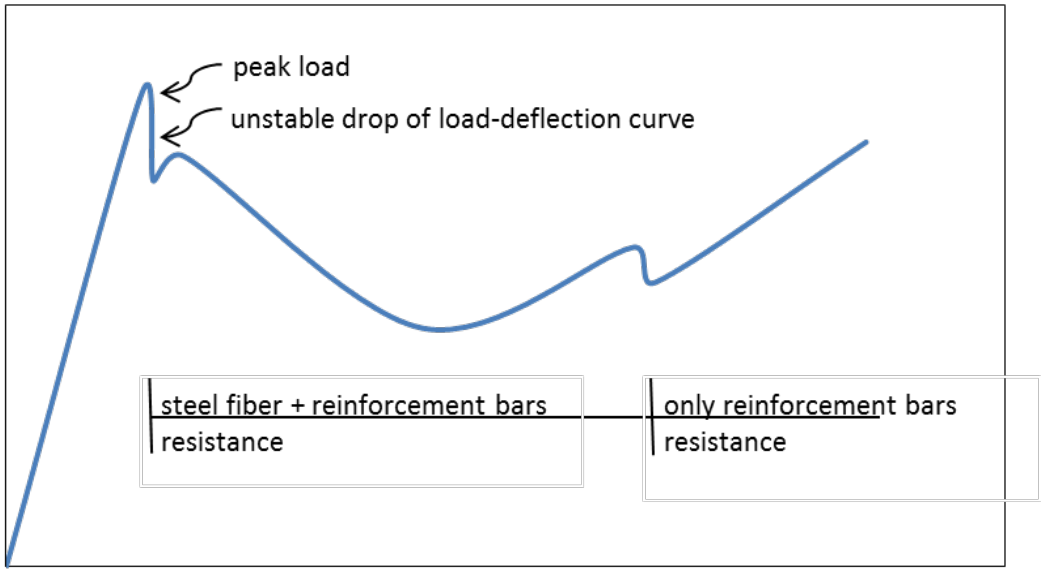

Fig. 4.2: Stages of load-bearing behavior of tested slabs

Table 4.1: Load and deflection characteristics of the tested slabs

Slab	G1Ufib0	G1Ufib0.5	G1Ufib1.1	G4Ut55	G3Uϱ1%	G2Nfc40	G5Ufy560
First crack load (kN)	64.7	79.38	168.08	26.20	56.4	40.32	78.12
First crack deflection (mm)	1.3	1.35	2.9	4.2	1.54	1.25	1.2
Service load (kN)	118.3	118.3	118.3	91	118.3	118.3	118.3
Service load deflection (mm)	2.5	1.95	1.93	18.52	3.4	4.10	2.1
Ultimate load (kN)	210.67	268.6	384.5	123.98	247.96	169.34	319.78
Ultimate load deflection (mm)	4.90	4.95	6.5	29.68	8.49	6.67	6.5

4.3 First Flexural Crack Load

Generally, the slab that failed under punching shear starts with flexural cracks and after a while the critical shear crack formed, so depending on variables adopted in this study, the ratio of first flexural crack load to the maximum load for each tested slab is presented in Table 4.2.

As expected for UHPC, increasing the fiber content increases the load at which the first cracking appears. Also when decreasing the thickness or the reinforcement ratio, the slab shows more flexural behavior and the first flexural crack starts at an earlier stage. When normal yield stress reinforcement was used, the slab shows dominant flexural behavior in comparison with the high strength steel bars. So, the decision to use high strength steel bars in this study to get pure punching shear type of failure could be justified.

It is important to mention that the first crack load of UHPC with 1.1 % steel fiber is four times higher than for the NSC slab. This can be attributed to the improved mechanical properties of UHPC.

The UHPC slab with 1.1% steel fiber (G1Ufib1.1) shows the maximum ratio of first flexural crack load to the maximum load which is about 43.7%, while the NSC slab (G2Nfc40) shows a ratio of only 23.8%. The thin UHPC slab with 55 mm thickness (G4Ut55) shows the lowest ratio of 21.1%.

Table 4.2: Ratio of first flexural crack load to the maximum load for tested slabs

Slab	Ratio of first flexural crack load to the maximum load	Maximum load (kN)
G1Ufib0	30.7%	210.6
G1Ufib0.5	29.5%	268.6
G1Ufib1.1	43.7%	384.5
G2Nfc40	23.8%	169.3
G3Uϱ1%	22.7%	247.9
G4Ut55	21.1%	123.9
G5Ufy560	24.4%	319.7

4.4 Opening of Critical Shear Crack

The failure of slabs under punching shear starts with the opening of the critical shear crack. This crack penetrates through the thickness of the slab to form the punching cone. Two cameras were used to follow the development of cracks and monitor the opening of the critical shear crack. The load at which the critical shear crack opened was therefore recorded. Table 4.3 shows the ratio of load at which the critical shear crack opened to the maximum load. From this, in the NSC slab, the critical shear crack is opened at a load of 71.7% from the maximum load while for the UHPC slab is between 65.3% and 86.3% from the maximum load depending on the variables adopted.

Table 4.3: Ratio of critical shear crack load to the maximum load for tested slabs

Slab	Ratio of critical shear crack load to the maximum load	Maximum load
G1Ufib0	-	210.6
G1Ufib0.5	81.5%	268.6
G1Ufib1.1	86.3%	384.5
G2Nfc40	71.7%	169.3
G3Uϱ1%	74.4%	247.9
G4Ut55	73.3%	123.9
G5Ufy560	65.3%	319.7

4.5 Comparison of Test Results

4.5.1 Fiber Content Effect

With regard to fiber content effect, three slabs of UHPC were considered, each with the same dimensions, compressive strength and reinforcement ratio. The only variable was fiber content, whereby the first slab G1Ufib0 had 0% fiber content, the second slab G1Ufib0.5 had 0.5%, while the third slab G1Ufib1.1 had 1.1% fiber content.

In comparison to the UHPC specimen without fibers, the deflection of the UHPC slab at service load decreases by 22.8% when 1.1% fibers were added. The load that caused the first crack in the tension area increased by 22.6% and by 159.7% when the fiber content was increased from 0% to 0.5% and 1.1% respectively. The punching load increased by 27.5% and 82.5% when the fiber content was raised from 0% to 0.5% and 1.1% respectively, see Table 4.1.

The addition of fibers leads to a decrease in deformations at all stages of loading, particularly after initial cracking, and enhances the maximum load carried by slab-column connection. Fibers not only delay the deformations of diagonal cracking within the slab, but also transfer the brittle type punching shear failure to a gradual and ductile shear failure.

4.5.2 Compressive Strength Effect

As already pointed out, the effect of compressive strength could be studied by comparing the UHPC slab G1Ufib0 (f_c=198.5 MPa) with the NSC slab G2Nfc40 (f_c= 40.3 MPa). All other parameters were kept constant. The load and deflection characteristics are described in Table 4.1.

At the service load stage, the deflection decreased by 39% when using UHPC instead of NSC. Furthermore, using UHPC in slab-column connection delays the appearance of the first crack and increases the first crack load by 60.4%. Increasing of punching load was expected when using UHPC instead of NSC. The amount of increase was 24.4%.

4.5.3 Reinforcement Ratio Effect

As for NSC, increasing the reinforcement ratio in UHPC increases the stiffness and decreases the deformations. In the service load stage, increasing the reinforcement ratio from 1% to 2% reduces the deflection by 42.6%, delays the appearance of the first crack, and increases the first crack load by 40.7%. The punching load was 8.3% higher; see Table 4.1. However, the effect of the reinforcement ratio on the punching shear strength of UHPC was expected to be higher than this value. Probably the reason is that the high strength steel bars used for constructing UHPC specimens did not have a pronounced rib deformation pattern.

4.5.4 Size Effect

In this variable two UHPC slabs were considered. The first slab (G4Ut55) had a thickness of 55 mm, and the second slab (G1Ufib0.5) a thickness of 100 mm, while all other variables of compressive strength, fiber content and reinforcement ratio were constant. The load and deflection characteristics can be seen in Table 4.1. The increase of thickness from 55 to 100 mm decreases the deflection by 89.4 % at service load stage, delays the appearance of the first crack, increases the first crack load by 202%, and increases the punching load by 116.6 %.

4.5.5 Yield Strength Effect

The effect of yield strength can be identified by comparing slab G5Ufy560 reinforced with normal yield strength bars of 562 MPa, to slab G1Ufib0.5 reinforced with high strength steel bars with an elastic limit of 1320 MPa.
It should be mentioned here that the UHPC slab with normal strength steel bars has a higher punching load (319.78 KN) in comparison with the slab of high strength bars (268.6 KN), see Table 4.1. This may be attributed to the effect of soft bond between the high strength steel bar and the concrete. The non-dimensional rib area of the normal steel bars is approximately 3.25 times that of the high strength steel bars.

4.6 Modes of Failure

Except slab G1Ufib0 (UHPC without steel fiber), all the slabs failed in punching shear as Figure 4.3 shows. The failure of all tested slabs started with flexural cracking located around the edges of the column in the tension area at load indicated in Table 4.2. These cracks were distributed in a radial and tangential direction to distances more than half the diameter of the cracked area. By increasing the imposed displacement incrementally, the flexural cracks increased in their width and moved toward the support till the critical shear crack formed at a load according to Table 4.3. Then the critical shear cracks distributed further through the slab to form the final shape of the punching shear cone. Figure 4.4 shows the flexural and shear cracks made after a radial section in the slab G5Ufy560.

For the UHPC slab without steel fibers (G1Ufib0), the failure started with the increase of the crack width near the supports in four sides, then from this area all the concrete cover gradually fell down with displacement increments. This type of failure is not punching shear but splitting of concrete cover mode due to the brittleness of UHPC without fibers; see Figure 4.3.

Interestingly, the tension surface of slabs G1Ufib1.1 and G5Ufy560 shows a trapezoidal deformation scheme when looking at a radial section through the plate. In order to study this finding in more detail, a cut was made in the slab G5Ufy560 along the line A-A shown in Figure 4.5. Not only the punching cone between shear cracks 2 and 3 can be seen, but also a secondary bending type mechanism with flexural hinges of the outermost part of the tension zone between points 1 and 2 as well as 3 and 4.

For slab G2Nfc40, the critical shear crack could not be recognized by the naked eye because the failure of this slab starts with the splitting of the concrete cover and then transfers to punching shear mode of failure; see Figure 4.3.

For the UHPC slab with 1% reinforcement ratio (G3Uϱ1%), the diameter of the punching shear cone in the tension area is larger than the other slabs. This is due to early yielding of tension reinforcement that shifted the failure perimeter far away from the center of the slab.

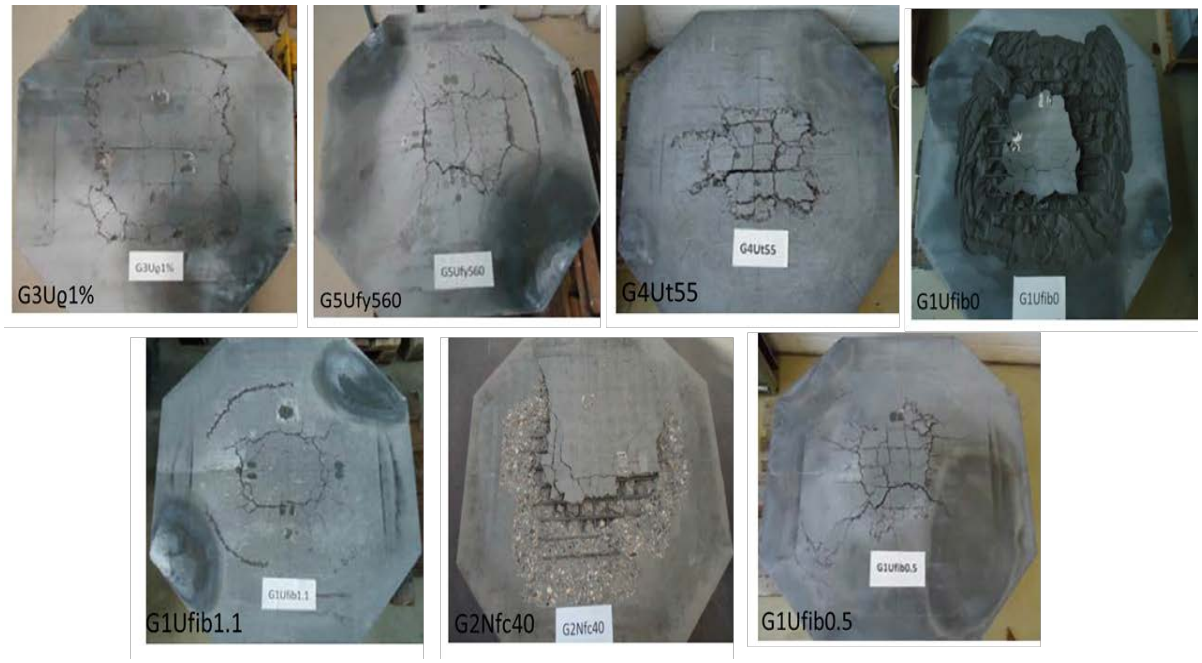

Fig. 4.3: Tested slabs' modes of failure

Fig. 4.4: Flexural and shear cracks

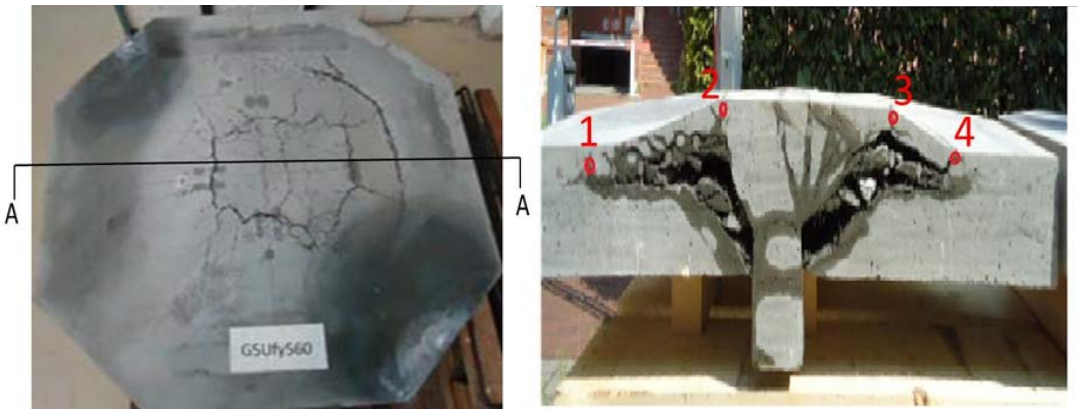

Fig. 4.5: Section A-A in slab G5Ufy560

Dowel action is defined as the capacity of reinforcement bars to resist the shear force which is perpendicular to the axis of tension reinforcement. When the dowel action takes place, the concrete around the reinforcement bars experiences progressive deterioration. The deflection of the dowel bars represents the relative displacement between the old and new positions of the deformed bar (Δd); see Figure 4.6.

Fig. 4.6: Deformation of reinforcement bars due to dowel action

4.7 Flexural Behavior of Tested Slab at the Time of Critical Shear Crack Opening

Figure 4.7 shows the flexural cracks that took place at the time of critical shear crack opening for each tested slab. The red lines represent the flexural cracks that took place, and the blue lines represent the location of the critical shear crack (first shear crack). The slabs G3Uϱ1%, G4Ut55, G5Ufy560 and G2Nfc40 showed dominant flexural behavior before the shear crack opened, and these slabs also have more radial cracks that moved to the edges of the slab.

UHPC slabs G1Ufib1.1 and G1Ufib0.5 show fewer flexural cracks before critical shear crack opening, especially the G1Ufib1.1 slab. UHPC slabs G4Ut55 and G3Uϱ1% have longitudinal cracks parallel to reinforcement which confirms the yielding of reinforcement near the area of column.

In the G1Ufib0 slab, the red lines represent the flexural cracks that appear before the split concrete cover mode of failure took place (there is no shear crack in this slab).

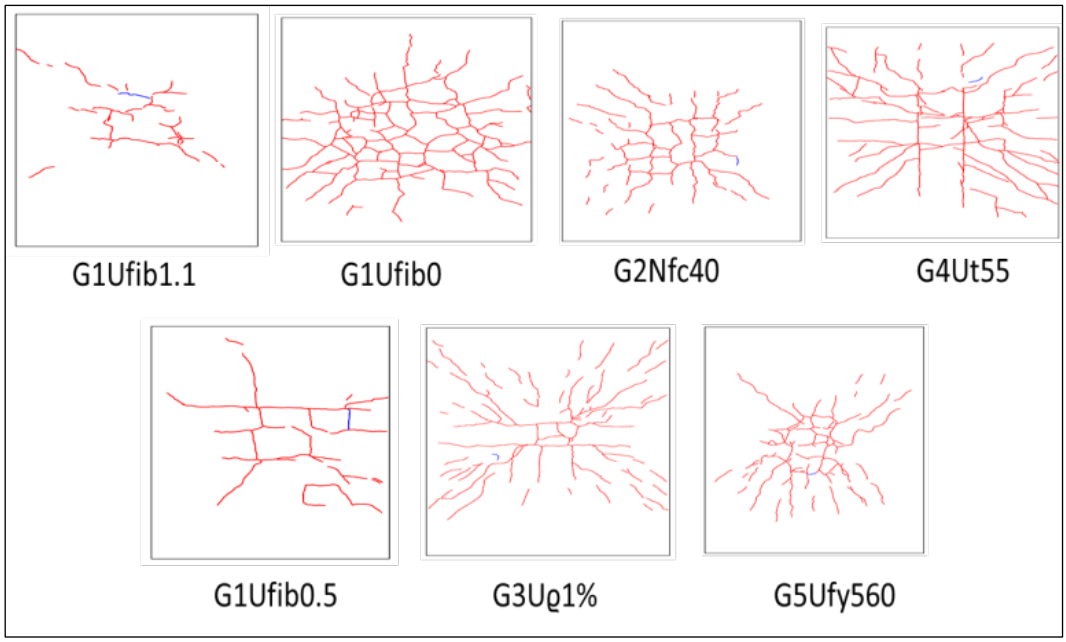

Fig. 4.7: Flexural cracks at the time of critical shear crack opening

4.8 Location of Critical Shear Crack and Angle of Punching Cone

An average of 16 points at the failure perimeter on the tension area measured from the center of the slabs were used to locate the critical shear crack on the tension surface and the angle of punching cone, as shown in Figure 4.8.

Figure 4.9 shows the distance from the center of the slab to the location of the critical shear crack for each tested slab. Figure 4.10 shows the punching cone angle for each tested slab.

From Figures 4.9 and 4.10, the slab G3Uϱ1% has the largest diameter of punching cone; this is due to early yielding of tension reinforcement shifting the shear cracks away from the face of the column. The NSC slab has the smallest punching diameter which may be due to aggregate interlock.

For the UHPC slab when the fiber content increased from 0.5% to 1.1%, the diameter of the punching cone reduced by 10.5%. Also for the UHPC slab when the value of thickness or reinforcement ratio was reduced or normal yield stress bars used, the slab shows dominant flexural behavior and consequently the diameter of the punching cone was larger. To compare between the UHPC slab of 0.5% and 1.1%

fiber content with the NSC slab, the diameter of the punching cone reduced by 4.6% and 14.6% when NSC was used instead of UHPC respectively.

The angle of the punching cone in Figure 4.10 is provided in degrees. For normal strength concrete (G2Nfc40) the angle of the punching cone is 30.3°, which is in agreement with the findings of other research. This angle becomes 29.1° for UHPC with 1.1% fiber content (G1Ufib1.1) and becomes 26.5° for UHPC with 0.5% fiber content (G1Ufib0.5). Also for UHPC when the thickness of the slab or reinforcement ratio is reduced, the angle also reduced to 11.9° and 16.8° respectively.

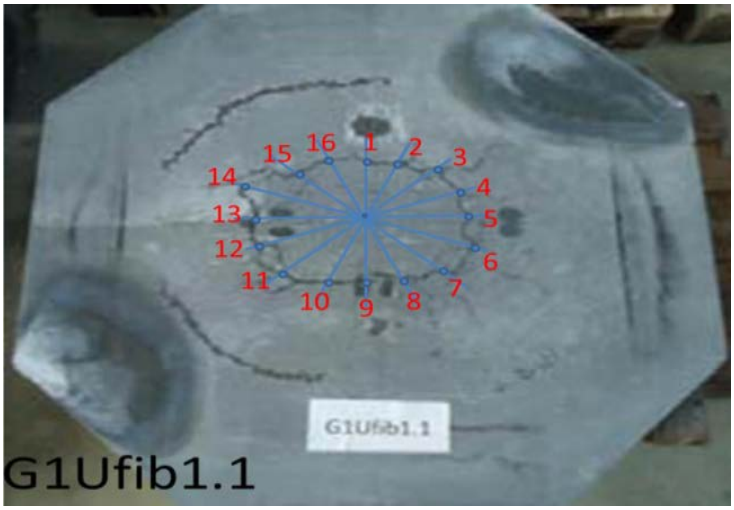

Fig. 4.8: Points to measure the location of shear crack and punching cone angle

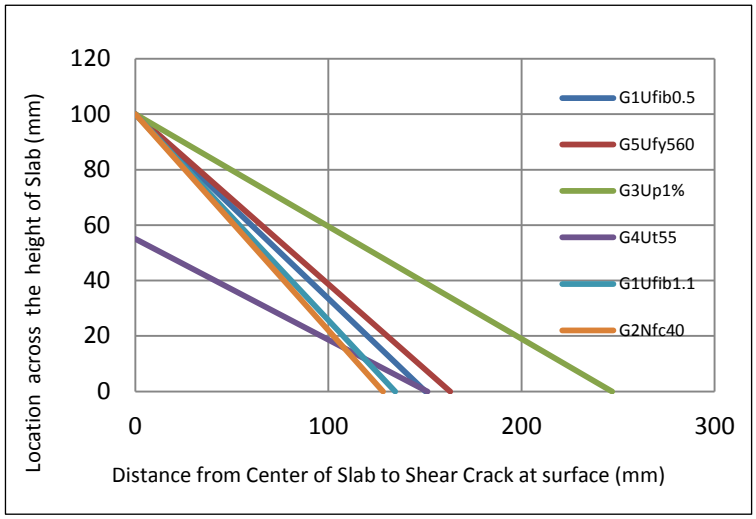

Fig. 4.9: Location of critical shear crack

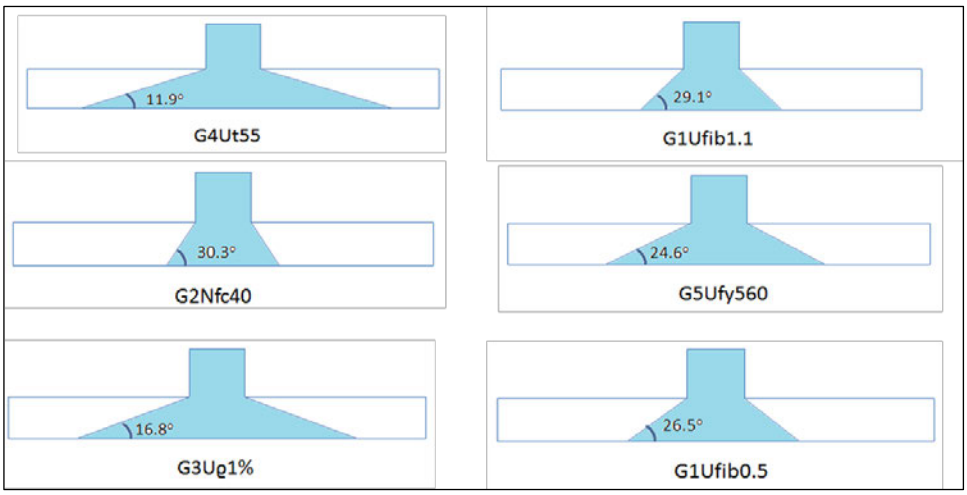

Fig. 4.10: Angle of punching cone for each tested slab

4.9 Critical Shear Perimeter

To design for punching shear, the first point to be considered is the definition of the critical shear perimeter. Generally, as the perimeter close to the loaded area is considered, the length of the perimeter rapidly gets shorter and hence the shear force per unit length of the perimeter rapidly increases.

On the basic form for the perimeter to be chosen, it is necessary to consider the distance from the column at which it should be located. The same load bearing capacity could be obtained by using a high value for shear strength combined with a short perimeter close to a column or by using a lower shear strength combined with a longer perimeter further from the column. Different codes adopted different critical shear perimeters. The DIN and UK code takes a perimeter of 1.5d from the face of the column; the ACI code uses a perimeter of 0.5d from the face of the column but with much higher stresses.

Observations of failure in experimental programs show that the failure perimeter at the tension surface takes the form of Figure 4.11 and it depends on the variables adopted. The idealization of shear perimeter at tension area according to DIN-1045-1 and EN 1992-1 was made and the final shape of the failure shear perimeter for the UHPC slabs is plotted in Figure 4.12.

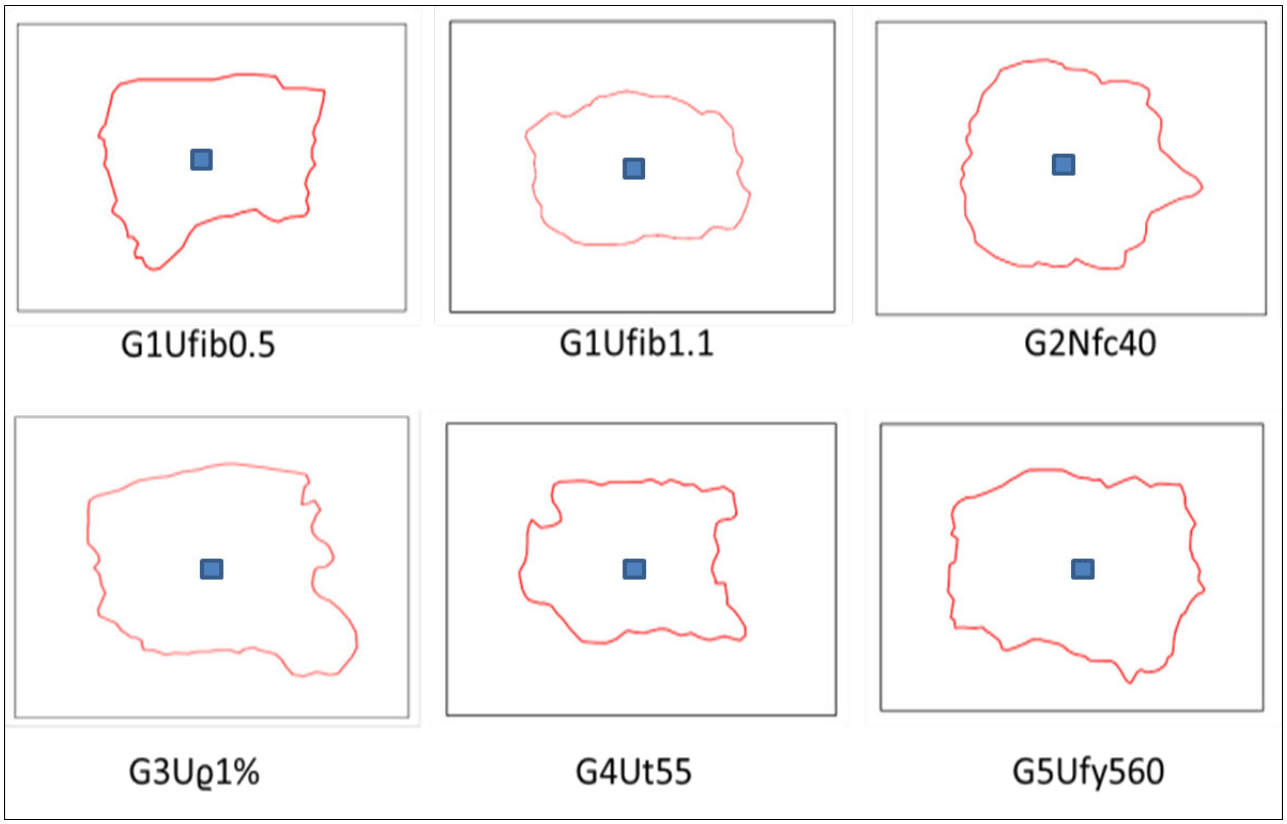

Fig. 4.11: Failure perimeter at tension surface for each tested slab

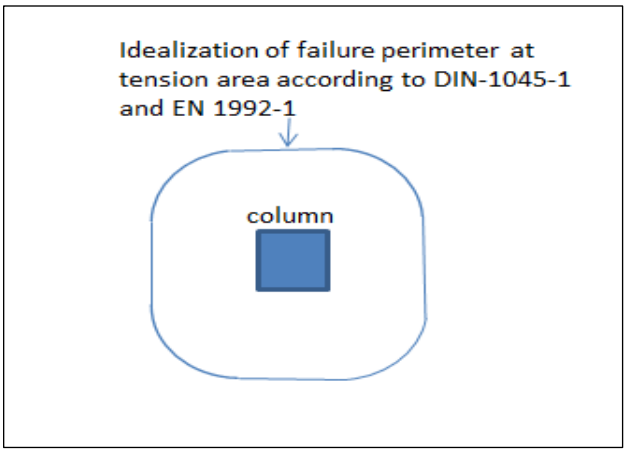

Fig. 4.12: Critical section perimeter of UHPC slabs

The failure shear perimeter and the critical shear section of the UHPC slab can be established from test data. With the band range of the variables, the average punching cone angle is 21.8°, the critical shear section located 1.25d from the face of the column and failure shear perimeter located 2.5d from the face of the column; see Figures 4.13 and 4.14.

So, for the UHPC slab; the proposed critical shear perimeter is:

$$\mathbf{b_o = 4c + 5\,\pi\,d} \qquad \text{.....(4.1)}$$

where:
b_o is the failure perimeter; c is the column dimension; and d is the effective depth of the slab.

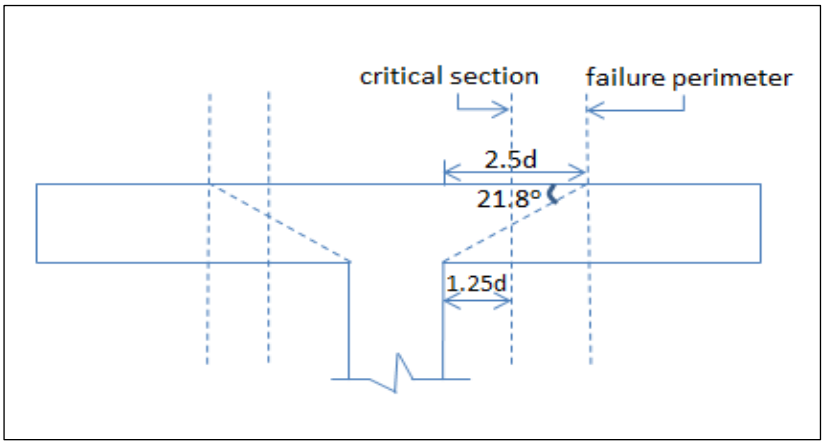

Fig. 4.13: Proposed critical shear section of UHPC slabs

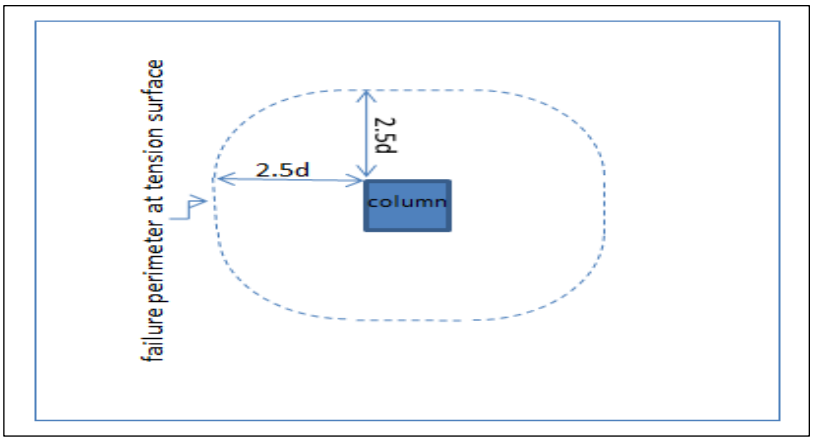

Fig. 4.14: Proposed failure perimeter of UHPC slab

4.10 Final Shape of Punching Cone

The camera used under the slab (in the tension area) helps to monitor the completion of the punching shear cone. Figure 4.14 shows the point in the load-deflection curve at which the final shape of the punching cone is completed. For all tested slabs the final shape of the punching cone is completed after the tension reinforcement starts to yield.

For the G4Ut55 slab, the final shape of the punching cone and the yielding of tension reinforcement take place at the peak load, while for other slabs it takes place after peak load and approximately at the lowest point of the softening load-deflection curve.

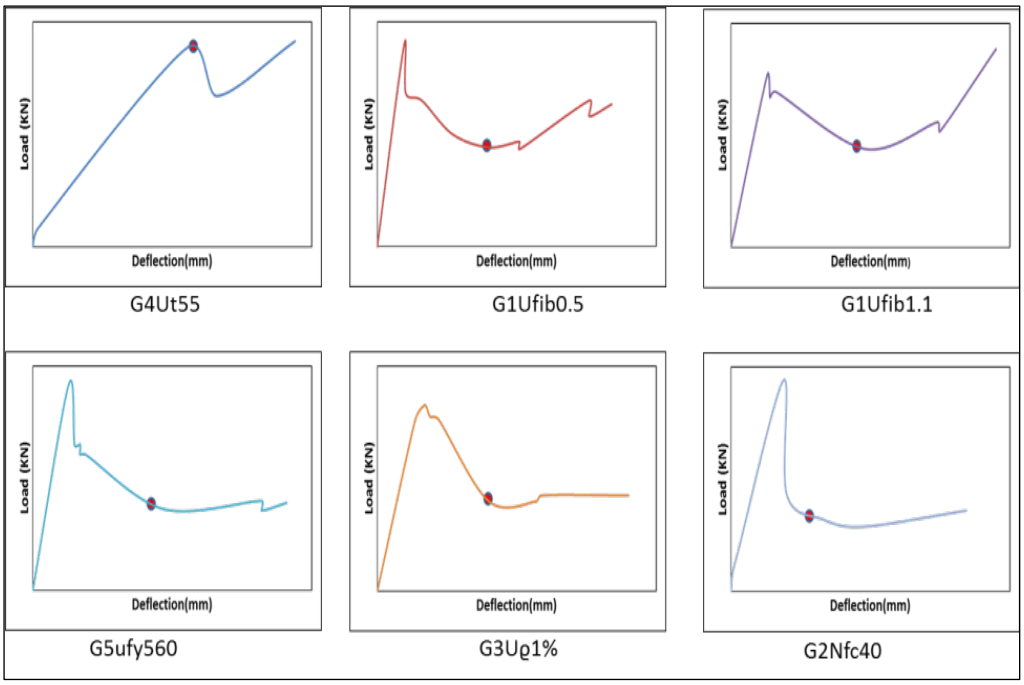

Fig. 4.14: Point in load-deflection curve at which the final shape of punching cone is completed

Chapter Five

Numerical and Analytical Analysis

5.1 Introduction

The finite element method is the most common numerical technique used in the field of engineering nowadays. By understanding concrete material properties, various concrete constitutive laws and failure criteria have been developed to model the behavior of concrete.

In this chapter, a feature of the finite element (FE) program used in this study to model the behavior of UHPC slabs under punching load is described. The FE model is followed by verification against experimental results of the reference slab G1Ufib0.5 (UHPC slab with 0.5% steel fiber), G1Ufib1.1% slab (UHPC with 1.1% steel fiber) and G2Nfc40 slab (normal strength concrete). Some variable effects on the punching shear behavior of slab-column connection are also demonstrated in a parametric study.

A proposal for design equation of UHPC slabs under punching load is presented and modified to include the HSC and NSC slabs without steel fibers.

5.2 Finite Element Analysis

Finite element analysis is a numerical technique used by engineers to find the solution for different problems. A fundamental assumption of the method states; that the domain can be divided into smaller regions in which the equations can be solved approximately. The region can also be divided into a finite number of elements, and the elements connected by nodes. By assembling the solution for each region, the behavior of all structures can be described.

In this study, the ATENA software program was used for the numerical modeling [14]. In ATENA, a 3D isoparametric element with 20 noded elements was used to represent the concrete of the slab close to the column; see Figure 5.1. The area of concrete far away from the column is represented by tetrahedral elements with 10 nodes; see Figure 5.2. Each node has three degrees of freedom.

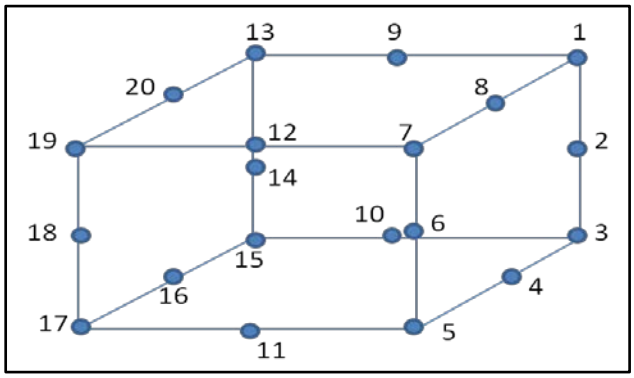

Fig. 5.1: 20-node brick elements

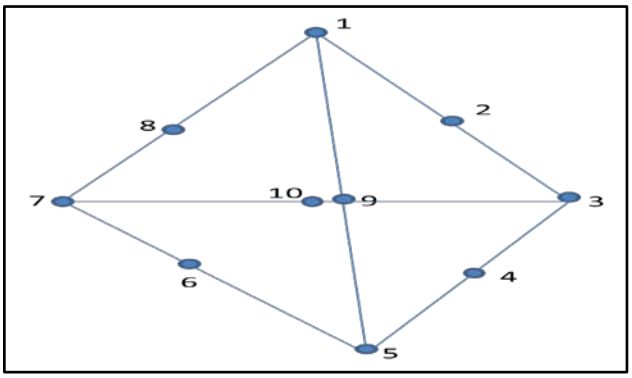

Fig. 5.2: 10-nodes tetrahedral elements

5.3 Material Modeling

The material model simulates the UHPC strain softening after both cracking and crushing. The uniaxial experimental test results of prisms, cylinders and reinforcement bars were used in the Finite Element Analysis (FEA).

Results gained from the FEA largely depend on material model and exterior boundary conditions. Nonlinear behavior of compression hardening and softening, fracture of concrete in tension based on nonlinear fracture mechanics, compressive strength reduction after tension cracking, shear retention factor, tension stress deterioration due to compression cracking, crack models and the simulation of tension reinforcement, were included in the material model.

Only a quarter of the slab was symmetrically modeled for numerical analysis. Redistribution of internal forces due to nonlinear material behavior was taken into account after each displacement increment, to satisfy forces equilibrium and deformations compatibility.

In order to simulate the material behavior of UHPC, CC3NonLinCementitious2User was chosen as material model, allowing users to define new laws for the material behavior. This model consists of a combined fracture-plastic constitutive model. Tension was handled by a fracture model based on Rankine failure criterion with a fixed crack model. A plasticity model for concrete in compression was modeled based on the Menétrey-Willam failure surface. The position of the Menétrey-Willam failure surface is not fixed, but can be expanded and moved along the hydrostatic axis simulating hardening and softening stages [14].

After the concrete is cracked, the tensile stress is released by strain softening behavior. The average tension softening law of uniaxial tensile test of prisms is used in the numerical analysis as tensile stress-displacement behavior. This is; normalizing with the characteristic length, which is equal to the projections of the finite element dimensions on the failure plane according to ATENA, to get the stress-strain relationship (see Figure 5.3).

The post-cracking behavior of UHPC in tension and the constitutive relationship depend on four parameters: matrix tensile strength (f_{tm}), width of the fracture process zone or characteristic length (l_{ch}), fracture energy (G_f), and shape of the softening diagram. The matrix tensile strength and the softening diagram were taken from the uniaxial tensile test of prisms. The fracture energy was calculated from the area under the stress-crack width curve of the uniaxial tensile test.

Both plain and reinforced concretes structure exhibit significant shear stiffness. The concrete's shear modulus reduced after cracking as the strain normal to the cracking grew. Across the cracks, the dowel action of steel bars contributes to the shear stiffness. The shear stiffness depends mainly on crack width and reinforcement ratio, whereby to include these effects, an appropriate value of shear modulus (G) must be used. In this study, the shear modulus for UHPC is kept constant till cracking takes place, then appropriate softening behavior in shear stiffness according to Fehling and Ismail [22] was adopted (see Figure 5.4).

As already pointed out, in the behavior of UHPC subject to multiaxial stresses, the Menétrey-Willam failure surface is adopted, as it satisfies the basic principles of continuum mechanics. The experimental uniaxial compressive strength of cylinders was used in the material model after normalizing the stress-displacement relationship to stress-strain relationship by dividing the displacement over the characteristic length, which is equal to 20 cm (length of concrete cylinder); see Figure 5.5.

In the case of flat slabs under punching load, a realistic modeling of reinforced concrete needs to consider multiaxial stress states not only uniaxial. The compressive strength of concrete can substantially decrease in relation to the uniaxial compressive strength to transverse stress and tension cracking. The reduction of compressive strength of UHPC after tension cracking in parallel direction to the cracks is computed in a similar way as in Fehling et al. [20] (see Figure 5.6). Also, the tensile strength of concrete can substantially decrease in relation to uniaxial tensile strength by increasing transverse compressive stress in relation to uniaxial compressive stress, according to the work of Grünberg et al. [25] (see Figure 5.7).

The bilinear stress-strain relationship with hardening is used to model the steel reinforcement as shown in Figure 5.8. The load was increased by deformation control in steps with the iterative solver of standard Newton-Raphson method.

In the nonlinear FEA of reinforced concrete structures, the smeared crack approach for modeling of the cracks is adopted within: fixed crack model and the rotated crack model. In both models the crack is formed when the principal stress exceeds the tensile strength. It is assumed that the cracks are uniformly distributed within the material volume [14].

Nonlinear analysis behavior can be classified according to type of non-linear behavior: first, nonlinear material behavior. This is the most common case for reinforced concrete structures. Because of the serviceability limitations, deformations are relatively small. Second, Deformations (either displacements or both displacements and rotations) are large enough such that the equilibrium equations must use the deformed shape of the structure. This non-linear analysis including both material and geometric equations is adopted here [14].

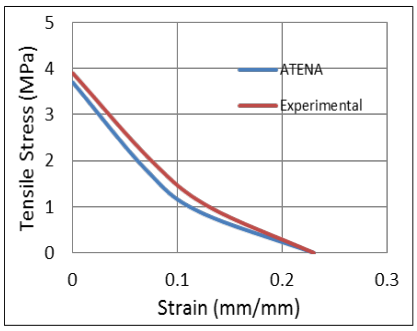

Fig. 5.3: ATENA and experimental tensile stress-strain curve

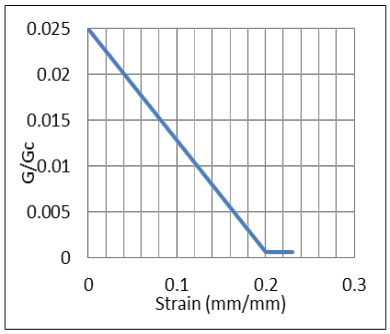

Fig. 5.4: Shear retention factor according to [21]

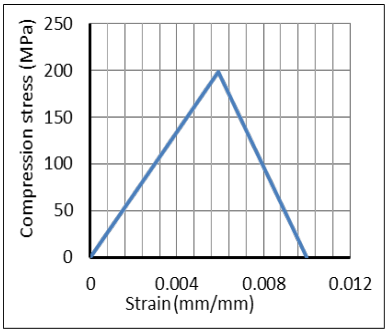

Fig. 5.5: Compression behavior of UHPC

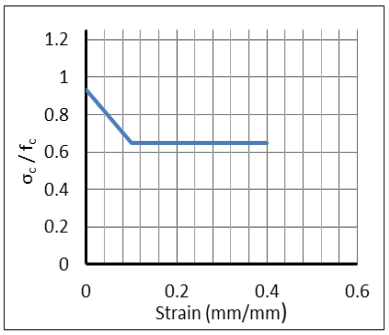

Fig. 5.6: Strength reduction in compression behavior of UHPC due to tension cracking

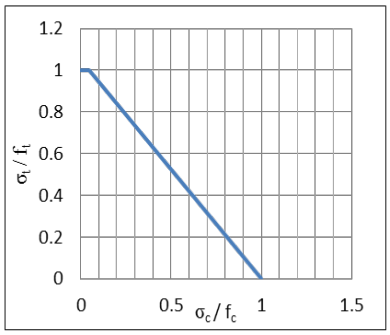

Fig. 5.7: Tensile stress deterioration due to transverse compressive stresses

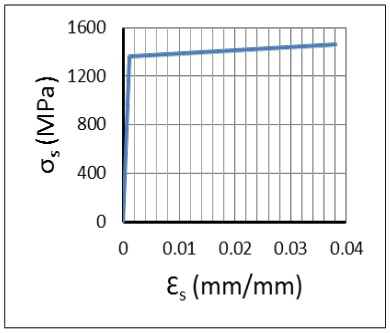

Fig. 5.8: Bilinear behavior with hardening stress-strain law for reinforcement

5.4 Calibration of Material Model in ATENA

To check the validity of the material model mentioned above, ATENA was calibrated with the uniaxial tension and compression test results. Figures 5.9 and 5.10 show a good agreement between the numerical and experimental results.

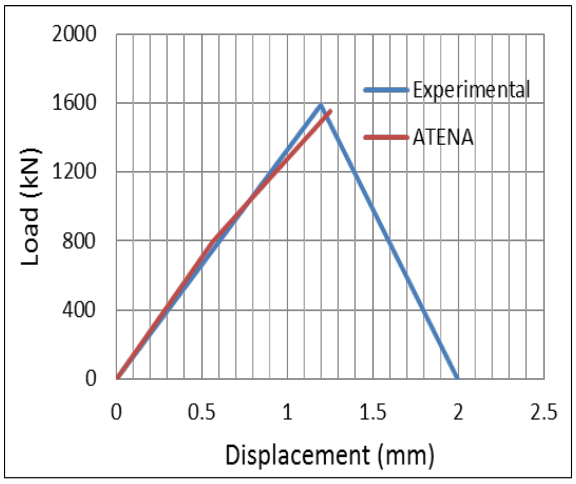

Fig. 5.9: Uniaxial compressive test for cylinder

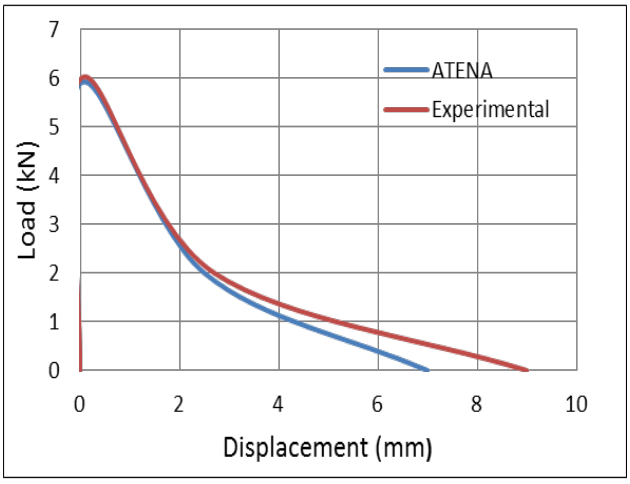

Fig. 5.10: Uniaxial tensile test of prism

5.5 Tension Stiffening Effect

In ATENA it is possible to reproduce the tension stiffening effect of reinforced concrete elements, including UHPFRC elements. This effect, which is a result of the post-cracking interaction of concrete and reinforcement, can be observed well when tension is applied to a single reinforcement bar embedded in a UHPC prism. Prior to concrete cracking, both concrete and reinforcement bar fully contribute to the stiffness of the specimen. Once the concrete starts to crack, its contribution decreases but the specimen stiffness is still higher than that of a bare reinforcement bar. This is due to concrete pieces between cracks constraining the bar elongation [15]; see Figure 5.11.

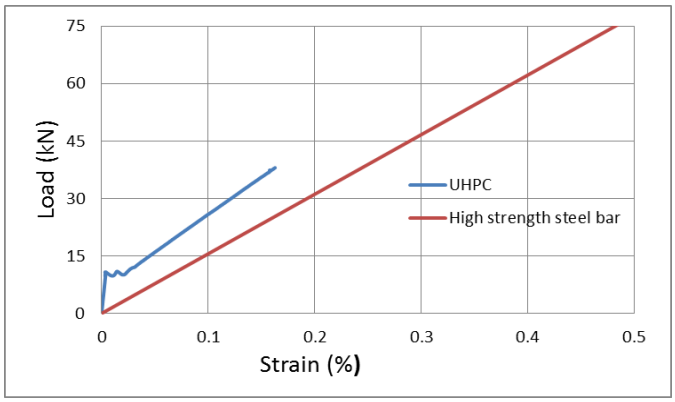

Fig. 5.11: Load-displacement curve of tension stiffening specimen for 0.5% fiber content

5.6 Geometric Slab Modeling

The tested slabs were simply supported along four edges and subjected to concentrated load at the center of the slab. Due to symmetry, a quarter of the slab was modeled for simplification. The punching failure zone was discretized into a fine mesh of brick elements. The load was applied on the slab by a deformation control through a steel plate with deformation step of 0.001 m. Figure 5.12 represents the model geometry used.

The punching zone was discretized with 0.05 m x 0.05 m x 0.05 m brick elements within an extension of 0.2 m from the center of the slab, and in the outer zone 0.1 m x 0.1 m x 0.1 m tetrahedral elements were used, in order to improve calculation time. Since the punching zone occurs near the column, there is no need to use fine mesh elements outside the punching area.

Due to the boundary conditions of the experimental tests, edges of the slab are free to lift along the line of contraflexure. Spring surface elements were used as

a support with stiffness zero in tension, and actual test setup stiffness in compression.

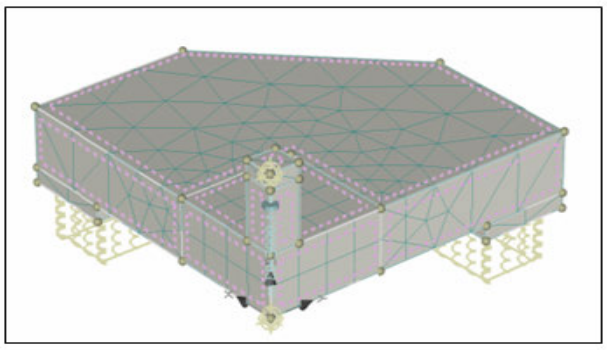

Fig. 5.12: Three dimensional flat slab model in ATENA

5.7 Boundary Conditions

To compare between the boundary conditions of the test setup at the lab and the boundary conditions of numerical analysis, an NSC slab (G2Nfc40) is considered in this numerical analysis. The material model of the G2Nfc40 slab was taken from the ATENA catalogue of concrete EC2 characteristic 40/45, and the geometrical modeling is the same as in Figure 5.12. Figure 5.13 shows the load-deflection curve of experimental and numerical analysis of slab G2Nfc40. The comparison between the numerical and experimental results is acceptable enough to agree with boundary conditions that will be used for numerical analysis of UHPC slabs.

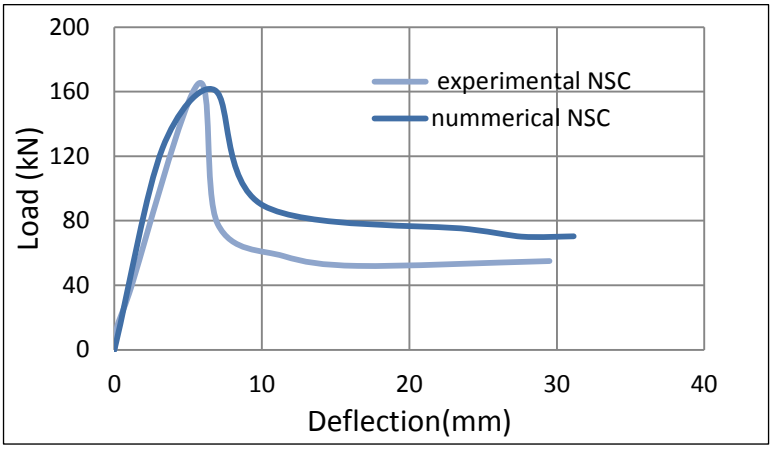

Fig. 5.13: Load-deflection curve of experimental and numerical of G2Nfc40 slab

5.8 Numerical Analysis of UHPC Slabs

5.8.1 Numerical Analysis of UHPC Slab with 0.5% Steel Fiber (G1Ufib0.5)

To verify the validity and accuracy of the adopted numerical model, and to check the ability of the constitutive model to simulate the behavior of UHPC slabs under punching load, the numerical result was compared with the experimental result for the reference slab G1Ufib0.5 (UHPC with 0.5% steel fiber). Through the ultimate punching load, the ratio of numerical to the experimental result is 0.99, which shows a good prediction of the adopted model. From Figure 5.14, it can be seen that the numerical load-deflection behavior before and after cracking follows the experimental results very closely up to 40% of the ultimate load. In the post peak range, the numerical load-deflection behavior is stiffer than the experimental result, which may be due to bending stiffness behavior of tension reinforcement in ATENA.

There is no meaningful difference between the experimental and numerical results in the descending part of the load-deflection curve because the numerical result also has stage of vertical drop in the load-deflection curve, a stage of combined resistance of tension reinforcement and steel fibers, and a stage of the pure tension reinforcement resistance as in experimental results.

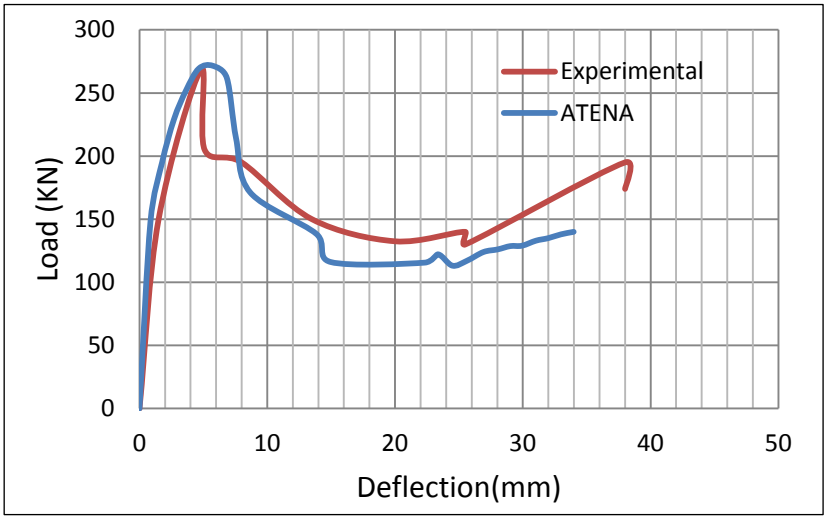

Fig. 5.14: Load-deflection curve of G1fib0.5 slab

5.8.2 Numerical Results of UHPC Slab with 1.1% Steel Fiber (G1Ufib1.1)

As already reported in the experimental study, the tested slabs have 0.5% and 1.1% fiber content, and afterwards the numerical model in ATENA was checked

for the NSC slab and for the UHPC slab with 0.5% steel fiber. In this section, the numerical model of UHPC slab with 1.1% steel fiber (G1Ufib1.1) is presented and compared with experimental results.
The parameters of the numerical material model of 1.1 % steel fiber are shown in Figures 5.15 to 5.20.

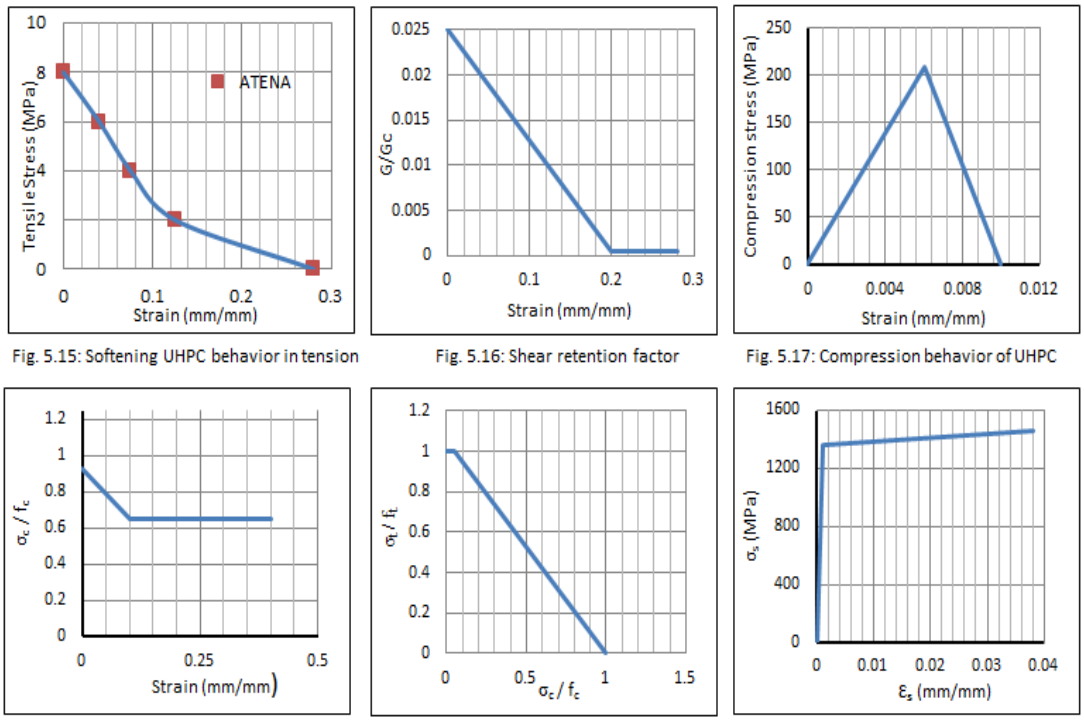

Fig. 5.15: Softening UHPC behavior in tension

Fig. 5.16: Shear retention factor

Fig. 5.17: Compression behavior of UHPC

Fig. 5.18: Strength reduction in compression behavior of UHPC due to tension cracking

Fig. 5.19: Tensile stress deterioration due to transverse compressive stresses

Fig. 5.20: Bilinear behavior with hardening stress-strain law for reinforcement

Figure 5.21 shows the numerical and experimental load-deflection curve of the G1Ufib1.1 slab, in which the ratio between numerical and the experimental punching load is 1.0. Also, the numerical result follows the experimental up to maximum load.

The softening behavior of the numerical result differs from that of the experimental result, but the numerical result shows that the slab failed also under punching shear. The strength of the tension reinforcement due to membrane action after the crushing of the concrete is also apparent in this numerical analysis.

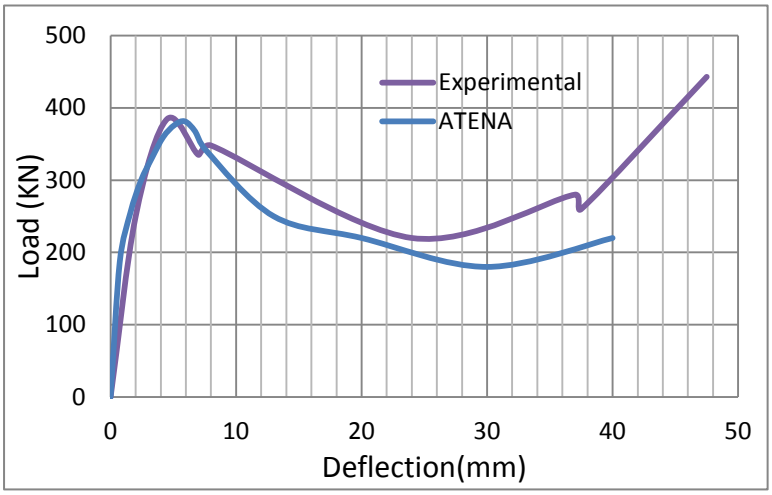

Fig. 5.21: Load-deflection curve of G1fib1.1slab

5.8.3 Sequence of Numerical Analyses

A sequence of numerical analyses was made to capture the experimentally tested slabs by changing numerically the parameters of reference slab G1Ufib0.5 to get the experimental punching load. In the numerical analysis, the thickness of the G1Ufib0.5 slab changed from 100 mm to 55 mm to get the experimental punching value of G4Ut55 (UHPC slab with 55 mm thickness). The reinforcement ratio of slab G1Ufib0.5 changed from 2% to 1% to get the experimental punching value of G3Uϱ1% (UHPC slab with 1% reinforcement ratio). Also the fibers content changed from 0.5% to 1.1% of reference slab G1Ufib0.5 with its material model to get the experimental punching result of G1Ufib1.1%. Table 5.1 shows the numerical and experimental results for the slabs that were tested experimentally.

Table 5.1: Experimental and numerical punching load for slabs tested at the lab

Name of experimentally tested slab	V_{exp} (kN)	V_{num} (kN)	V_{exp} / V_{num}
G1Ufib0.5	268.6	271.6	0.99
G3Uϱ1%	247.9	253.2	0.97
G4Ut55	123.9	115.3	1.07
G1Ufib1.1	384.5	381.9	1.00

5.9 Parametric Analysis

A very good match in punching load between numerical and experimental results helps to study the factors' effect on punching shear strength of slab-column connection through a parametric analysis. This parametric analysis helps to get more insight although the number of experimental test specimens was limited due to the high costs. The G1Ufib0.5 slab is taken as a reference in this parametric analysis.

5.9.1 Influence of Post Cracking Fiber Efficiency

The influence of fiber efficiency on punching shear was studied by changing the references fiber efficiency of slab G1Ufib0.5 (v_{fte} = 3.9 MPa) with the values ranging from 1 MPa to 14 MPa, see Table 5.2. By keeping other variables constant and increasing the fiber efficiency of tensile strength to 14 MPa, the punching load was increased from 271.6 to 426.6 kN. When the fiber efficiency of tensile strength decreased to 1 MPa, the punching load decreased from 271.6 to 187.1 kN. Figure 5.22 shows the load-deflection curve for values of fiber efficiency.

It is shown in Figure 5.23 that the punching shear strength increases with fiber efficiency of tensile strength by a 0.35 power function. The increase of punching load due to increase tensile strength was expected, because concrete punching strength is determined roughly by tensile resistance at the inclined shear crack.

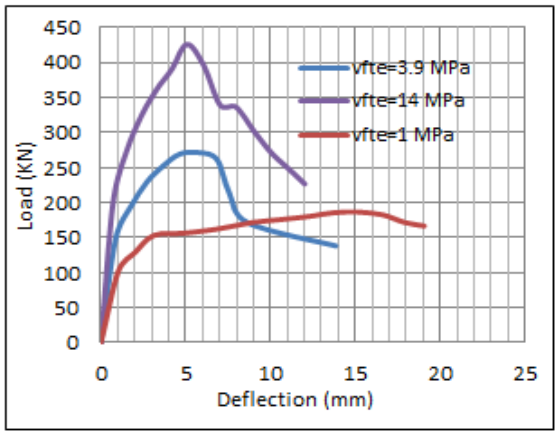

Fig. 5.22: load-deflection curve for different efficiency tensile strength

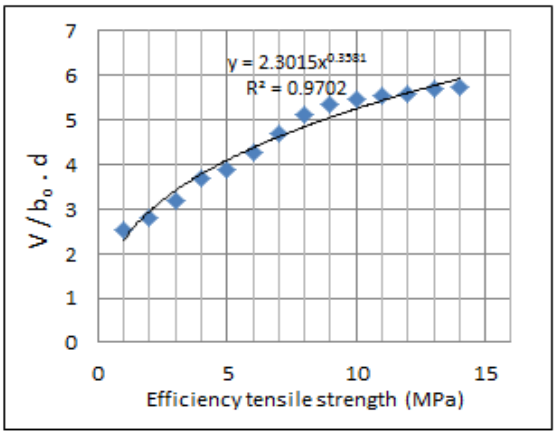

Fig. 5.23: Influence function of efficiency tensile strength on punching shear

Table 5.2: Numerical punching loads for different values of fiber efficiency

No. of slab	f_c (MPa)	100	h	fiber efficiency, v_{fte} (MPa)	fiber content (%)	V_{num} (kN)
1	198.6	2	100	1	0.1	187.1
2	198.6	2	100	2	0.24	208.3
3	198.6	2	100	3	0.374	235.5
4	198.6	2	100	4	0.51	273.3
5	198.6	2	100	5	0.65	287.2
6	198.6	2	100	6	0.79	317.1
7	198.6	2	100	7	0.93	348.6
8	198.6	2	100	8	1.1	381.9
9	198.6	2	100	9	1.21	397.4
10	198.6	2	100	10	1.35	405.2
11	198.6	2	100	11	1.49	410.1
12	198.6	2	100	12	1.63	415.3
13	198.6	2	100	13	1.77	422.4
14	198.6	2	100	14	1.96	426.6

5.9.2 Influence of Compressive Strength

The values ranging from 150 MPa to 250 MPa and were used to study the effect of compressive strength of UHPC on punching shear; see Table 5.3, starting by taking f_c =199 MPa as a reference for the compressive strength of slab G1Ufib0.5. Increasing the compressive strength from 199 MPa to 250 MPa, will increase the punching load from 271.6 to 296.2 kN, while decreasing the compressive strength from 199 MPa to 150 MPa, will decrease the punching load from 271.6 to 245.1 kN. Figure 5.24 shows the load-deflection curve for 150, 199 and 250 MPa compressive strength.

Also, it is shown in Figure 5.25 that the punching strength increase approximately follows a power function of 0.35 of the compressive strength. This result is close to the provisions of DIN-1045 (power function of 1/3), but it does not match with the ACI-318 provisions (power function of 1/2) for NSC.

This factor has a significant effect on punching shear, because the punching

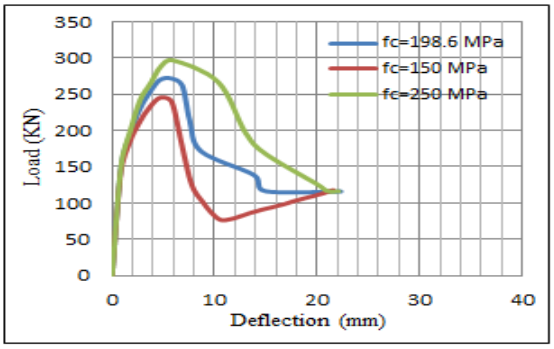

Fig. 5.24: load-deflection curve for different compressive strength

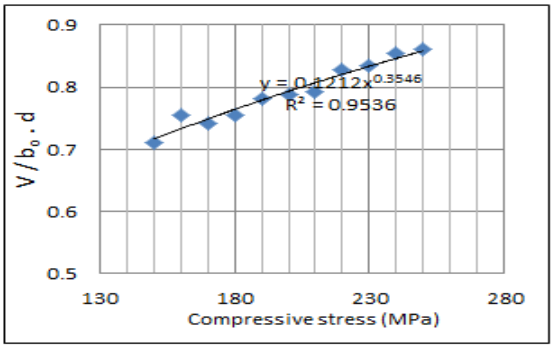

Fig. 5.25: Influence function of compressive strength on punching shear

failure depends mainly on the high stress compressive zone and the load transferred to the column by an inclined strut.

Table 5.3: Numerical punching loads for different compressive strengths

No. of slab	f_c (MPa)	100ϱ	h (mm)	Fiber efficiency, v_{fte} (MPa)	Fiber content (%)	V_{num} (kN)
1	150	2	100	3.9	0.5	245.1
2	160	2	100	3.9	0.5	260.2
3	170	2	100	3.9	0.5	255.5
4	180	2	100	3.9	0.5	260
5	190	2	100	3.9	0.5	269.3
6	198.6	2	100	3.9	0.5	271.6
7	210	2	100	3.9	0.5	273.4
8	220	2	100	3.9	0.5	285.2
9	230	2	100	3.9	0.5	287
10	240	2	100	3.9	0.5	294.1
11	250	2	100	3.9	0.5	296.2

5.9.3 Influence of Reinforcement Ratio

The influence of the tension reinforcement ratio on punching strength was studied by replacing the reference reinforcement ratio of 2% of slab G1Ufib0.5 with the values ranging from 0.1% to 2.9%; see Table 5.4. Increasing the reinforcement ratio from 2% to 2.9% will increase the punching load from 271.6 to 283.2 kN, while decreasing the reinforcement ratio from 2% to 0.1%, will decrease the punching load from 271.6 to 139 kN. Figure 5.26 shows the load-deflection curve for different reinforcement ratios.

The punching resistance can be described approximately by a 0.21 power functions of the reinforcement ratio; see Figure 5.27. In NSC, the increase in punch-

ing strength with increased reinforcement ratio has a power function of (1/3) according to DIN-1045-1 and is not included in the ACI-318 code of practice.
Shear strength was expected to increase with increased reinforcement ratio also due to the dowel effect. Also, the increase in tension reinforcement ratio increases the height of the compression zone leading to higher punching loads accompanied by more brittle failure.

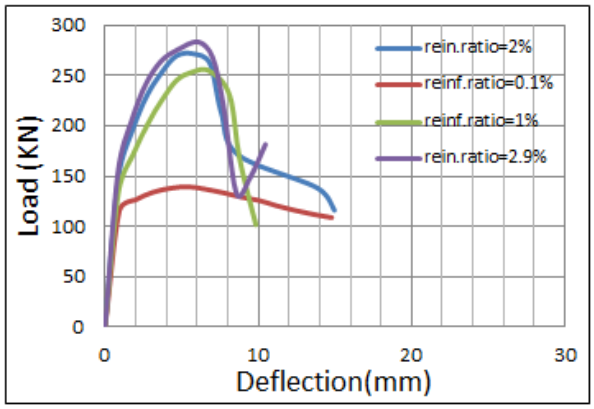

Fig. 5.26: load-deflection curve for different reinforcement ratio

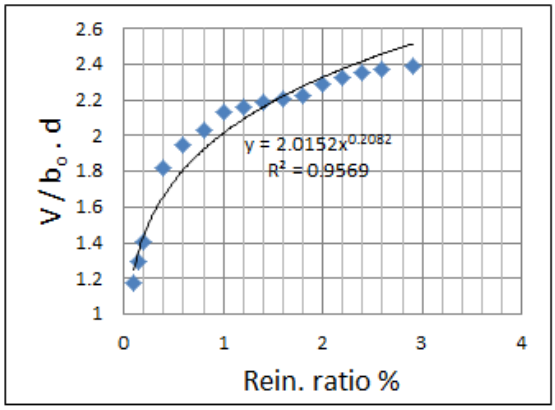

Fig. 5.27: Influence function of reinforcement ratio on punching shear

Table 5.4: Numerical punching loads for different reinforcement ratios

No. of slab	f_c (MPa)	100ϱ	h (mm)	Fiber efficiency, v_{fte} (MPa)	fiber content (%)	V_{num} (kN)
1	198.6	0.1	100	3.9	0.5	155
2	198.6	0.2	100	3.9	0.5	166
3	198.6	0.4	100	3.9	0.5	215.1
4	198.6	0.6	100	3.9	0.5	231
5	198.6	0.8	100	3.9	0.5	240.2
6	198.6	1	100	3.9	0.5	253.2
7	198.6	1.2	100	3.9	0.5	256.7
8	198.6	1.4	100	3.9	0.5	259
9	198.6	1.6	100	3.9	0.5	261.1
10	198.6	1.8	100	3.9	0.5	263.1
11	198.6	2	100	3.9	0.5	271.6
12	198.6	2.2	100	3.9	0.5	275.3
13	198.6	2.4	100	3.9	0.5	278.5
14	198.6	2.6	100	3.9	0.5	281.1
15	198.6	2.9	100	3.9	0.5	283.2

5.9.4 Size Effect

The values ranging from 40 mm to 300 mm were used to study the effect of thickness of UHPC slabs on punching shear; see Table 5.5. As already mentioned, the reference slab G1Ufib0.5 has a thickness of 100 mm. By increasing the thickness of the slab to 300 mm, the punching load increases from 271.6 to 1330 kN. Also the punching load decreases from 271.6 to 74 kN when the thickness of slab decreases to 40 mm. Figure 5.28 shows the load-deflection curve for different slab thickness.

Figure 5.29 shows the 0.85 power function increasing of punching strength with increased slab thickness. For NSC, this relation has a form of $(1+\sqrt{200/d})$ according to DIN-1045, which is very close to the present study size effect relation. The ACI-318 code does not include this factor in their formula.

According to Figure 5.30, the punching load increased with increasing slab thickness. The significant effect of slab size on punching shear is due to the fact that increasing the size of the slab increased the strain energy release to the fracture zone, thus more fracture energy is needed for failure.

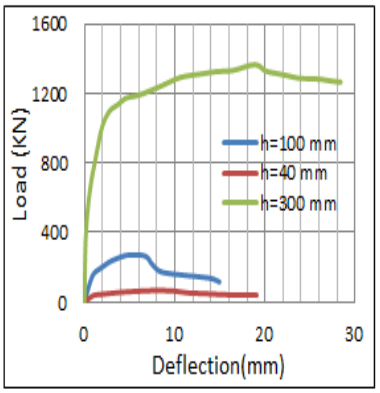

Fig. 5.28: load-deflection curve for different slab thickness

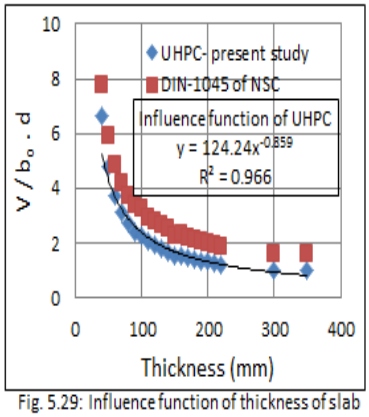

Fig. 5.29: Influence function of thickness of slab on punching shear

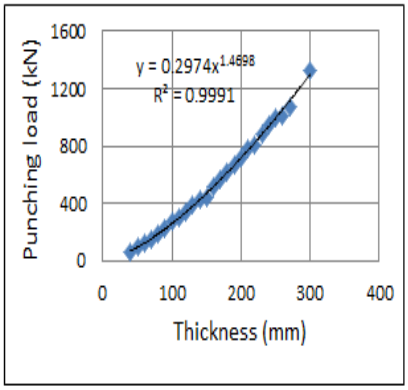

Fig. 5.30: Influence function of size of slab on punching load

Table 5.5: Numerical punching loads for different slab thicknesses

No. of slab	f_c (MPa)	100ϱ	h (mm)	Fiber efficiency, v_{fte} (MPa)	fiber content (%)	V_{num} (kN)
1	198.6	2	40	3.9	0.5	74
2	198.6	2	50	3.9	0.5	97.8
3	198.6	2	60	3.9	0.5	123.3
4	198.6	2	70	3.9	0.5	154.6
5	198.6	2	80	3.9	0.5	188.2
6	198.6	2	90	3.9	0.5	223.7
6	198.6	2	100	3.9	0.5	271.6
7	198.6	2	110	3.9	0.5	300.5
8	198.6	2	120	3.9	0.5	341.5
9	198.6	2	130	3.9	0.5	384.2
10	198.6	2	140	3.9	0.5	428.4
11	198.6	2	150	3.9	0.5	445
12	198.6	2	160	3.9	0.5	521.4
13	198.6	2	170	3.9	0.5	570
14	198.6	2	180	3.9	0.5	619.9
15	198.6	2	190	3.9	0.5	671.2
16	198.6	2	200	3.9	0.5	723.8
17	198.6	2	210	3.9	0.5	777.6
18	198.6	2	220	3.9	0.5	806.2
19	198.6	2	230	3.9	0.5	877.1
20	198.6	2	240	3.9	0.5	945.6
21	198.6	2	250	3.9	0.5	992.5
22	198.6	2	260	3.9	0.5	1010.1
23	198.6	2	270	3.9	0.5	1077.4
24	198.6	2	300	3.9	0.5	1330.2

5.10 Proposed Design Equation

A design equation for UHPC slabs under punching load is proposed based on the work of Narayanan and Darwish [56] for punching shear strength of NSC with steel fiber. The reason for choosing this model and developing it to UHPC was that Narayanan and Darwish believed that no appreciable amount of shear force was expected to be carried by aggregate interlock across the cracks as the specimens did not include any coarse aggregate.

Narayanan and Darwish considered that the punching shear strength of concrete consists of contributions of:

- The strength of the very narrow compressive zone above the top of the inclined cracks;
- The pull-out forces on the fibers along inclined cracks; and
- The shear force carried by the dowel and membrane actions which contribute the shear capacity.

For the same basic idea used by Narayanan and Darwish but using the full fiber efficiency of tensile strength along the inclined shear cracks instead of pull-out forces on the fibers along inclined cracks, the new form of the present design equation is as follows:

$$v_{pro} = (v_{fc} + v_{fte} + v_{\varrho}) \quad \text{.....(5.1)}$$

where:

v_{pro} is the proposed shear strength of the UHPC slab
v_{fc} is the shear resistance of the very narrow compression zone above the top of the inclined cracks
v_{fte} is the full fiber efficiency of tensile strength along the inclined shear cracks and;
v_{ϱ} is the shear strength carried by the dowel and membrane actions

Including the size effect and modifying the failure perimeter by the fiber factor (F), Equation 5.1 will be:

$$V_{pro} = 0.35[\beta_d (v_{fc} + v_{fte} + v_{\varrho}) b_{of} d] \quad \text{.....(5.2)}$$

with:

$$v_{fc} = 0.12 (f_c)^{0.35} \quad \text{.....(5.3)}$$

$$\beta_d = 125/d^{0.87} \quad \text{.....(5.4)}$$

$$v_{\varrho} = (100\varrho)^{0.21} \quad \text{.....(5.5)}$$

$$b_{of} = b_o (1 - KF) \quad \text{.....(5.6)}$$

$$F = (L / D) V_f D_f \quad \text{.....(5.7)}$$

Where:

- 0.35 is the constant from statistical analysis
- β_d is the size effect factor

- f_c is the cylindrical compressive strength (MPa)
- d is the average effective depth (mm)
- ϱ is the tension reinforcement ratio
- b_o is the reference critical failure perimeter from Equation 4.1
- b_{of} is the modified critical failure perimeter taking into account the fiber content effect according to [56]
- F is the fiber factor, K is the non-dimensional constant value (= 0.45)
- V_f is the fiber volume fraction
- D_f is the bond factor for NSC adopted here (0.5 for round fiber, 0.75 for crimped fibers and 1.0 for duoform fibers), and
- L and D are the length and diameter of fiber (mm) respectively

The functions of the factors; size effect, reinforcement ratio, compressive strength and fiber efficiency of tensile strength in the proposed design equation were taken from the parametric analysis in section 5.8.
From experimental measurements in section 4.8, the distance from the center of the tested slab to the shear crack is already reported. By comparing the maximum and minimum position of the critical shear crack for all tested slabs, the non-dimensional factor (K) is set to 0.45.

5.11 Comparison of Design Equation with Numerical Results

The proposed design equation was applied on 63 UHPC slabs numerically analyzed in parametric analysis (see section 5.9), and the results presented in Table 5.6 and Figure 5.32 in order to verify the accuracy. The proposed design equation is shown to be applicable for a wide range of parametric variations; ranging between 40 mm and 300 mm in slab thickness, 0.1 % and 2.9 % in tension reinforcement ratio, 150 MPa and 250 MPa in compressive strength of concrete and 0.1 % to 1.96 % fiber content with fiber efficiency of tensile strength ranging from 1 MPa to 14 MPa respectively.

Table 5.6: Numerical and proposed punching shear loads

No. of slab	f_c (MPa)	100ϱ	h (mm)	v_{fte} (MPa)	Fiber content (%)	V_{num} (kN)	V_{pro} (kN)	V_{num} / V_{pro}
1	150	2	100	3.9	0.5	245.1	245.4	0.99
2	160	2	100	3.9	0.5	260.2	288.1	0.90
3	170	2	100	3.9	0.5	255.5	289.8	0.88
4	180	2	100	3.9	0.5	260	291.4	0.89
5	190	2	100	3.9	0.5	269.3	292.9	0.91
6	198.6	2	100	3.9	0.5	271.6	294.2	0.92
7	210	2	100	3.9	0.5	273.4	295.9	0.92
8	220	2	100	3.9	0.5	285.2	297.3	0.95
9	230	2	100	3.9	0.5	287	298.7	0.96
10	240	2	100	3.9	0.5	294.1	300.0	0.98
11	250	2	100	3.9	0.5	296.2	301.3	0.98
12	198.6	0.1	100	3.9	0.5	155	234.8	0.66
13	198.6	0.2	100	3.9	0.5	166	245.4	0.67
14	198.6	0.4	100	3.9	0.5	215.1	257.7	0.83
15	198.6	0.6	100	3.9	0.5	231	265.8	0.86
16	198.6	0.8	100	3.9	0.5	240.2	271.9	0.88
17	198.6	1	100	3.9	0.5	253.2	277.0	0.91
18	198.6	1.2	100	3.9	0.5	256.7	281.3	0.91
19	198.6	1.4	100	3.9	0.5	259	285.0	0.90
20	198.6	1.6	100	3.9	0.5	261.1	288.4	0.90
21	198.6	1.8	100	3.9	0.5	263.1	291.5	0.90
22	198.6	2.2	100	3.9	0.5	275.3	296.8	0.92
23	198.6	2.4	100	3.9	0.5	278.5	299.2	0.93
24	198.6	2.6	100	3.9	0.5	281.1	301.5	0.93
25	198.6	2.9	100	3.9	0.5	283.2	304.6	0.92
26	198.6	2	40	3.9	0.5	74	96.1	0.76
27	198.6	2	50	3.9	0.5	97.8	128.1	0.76
28	198.6	2	60	3.9	0.5	123.3	160.4	0.76
29	198.6	2	70	3.9	0.5	154.6	193.1	0.80
30	198.6	2	80	3.9	0.5	188.2	226.3	0.83
31	198.6	2	90	3.9	0.5	223.7	260.1	0.86
32	198.6	2	110	3.9	0.5	300.5	328.8	0.91
33	198.6	2	120	3.9	0.5	341.5	363.8	0.93
34	198.6	2	130	3.9	0.5	384.2	399.2	0.96
35	198.6	2	140	3.9	0.5	428.4	434.9	0.98
36	198.6	2	150	3.9	0.5	445	471.0	0.94
37	198.6	2	160	3.9	0.5	521.4	507.3	1.02
38	198.6	2	170	3.9	0.5	570	544.0	1.04
39	198.6	2	180	3.9	0.5	619.9	580.9	1.06
40	198.6	2	190	3.9	0.5	671.2	618.1	1.08
41	198.6	2	200	3.9	0.5	723.8	655.5	1.10
42	198.6	2	210	3.9	0.5	777.6	693.2	1.12

43	198.6	2	220	3.9	0.5	806	731.2	1.10
44	198.6	2	230	3.9	0.5	870.1	769.3	1.13
45	198.6	2	240	3.9	0.5	928.6	807.7	1.16
46	198.6	2	250	3.9	0.5	986.2	846.3	1.17
47	198.6	2	260	3.9	0.5	986.3	885.1	1.14
48	198.6	2	270	3.9	0.5	986.5	924.0	1.16
49	198.6	2	300	3.9	0.5	1330.2	1042.1	1.27
50	198.6	2	100	1	0.1	187.1	239.2	0.78
51	198.6	2	100	2	0.24	208.3	255.2	0.81
52	198.6	2	100	3	0.374	235.5	274.5	0.85
53	198.6	2	100	4	0.51	273.3	296.1	0.92
54	198.6	2	100	5	0.65	287.2	319.3	0.89
55	198.6	2	100	6	0.79	317.1	343.2	0.92
56	198.6	2	100	7	0.93	348.6	367.3	0.94
57	198.6	2	100	8	1.1	381.9	394.1	0.96
58	198.6	2	100	9	1.21	397.4	414.3	0.95
59	198.6	2	100	10	1.35	405.2	436.6	0.92
60	198.6	2	100	11	1.49	410.1	457.9	0.89
61	198.6	2	100	12	1.63	415.3	478.0	0.86
62	208.2	2	100	13	1.77	422.4	496.5	0.85
63	150	2	100	14	1.96	426.6	515.7	0.82
						Mean Value		0.98

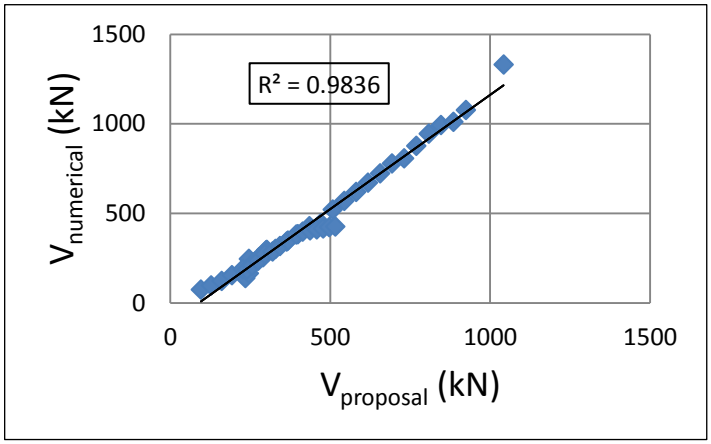

Fig. 5.32: Comparison of punching loads predicted from numerical model (section 5.9) and proposed design formula (section 5.10)

It is observed that the prediction of the proposed design equation generally gives very satisfactory predictions of UHPC punching shear strength, with R^2 =0.98 and mean value ratio=0.98.

To check again the relation of experimental to numerical punching loads (Table 5.6), and experimental to proposal punching loads (Eq.5.2) for the slabs tested at the lab; Table 5.7 and Figure 5.33 show the following ratios.

Table 5.7: The experimental, numerical and proposal punching loads for slabs tested at the lab

Name of experimental tested slabs	V_{exp} (kN)	V_{num} (kN)	V_{pro} (kN)	V_{exp} / V_{num}	V_{exp} / V_{pro}
G1Ufib0.5	268.6	271.6	294.2	0.98	0.91
G3Uϱ1%	247.9	253.2	277.0	0.97	0.89
G4Ut55	123.9	110.5	144	1.12	0.86
G1Ufib1.1	384.5	381.9	394.1	1.0	0.97

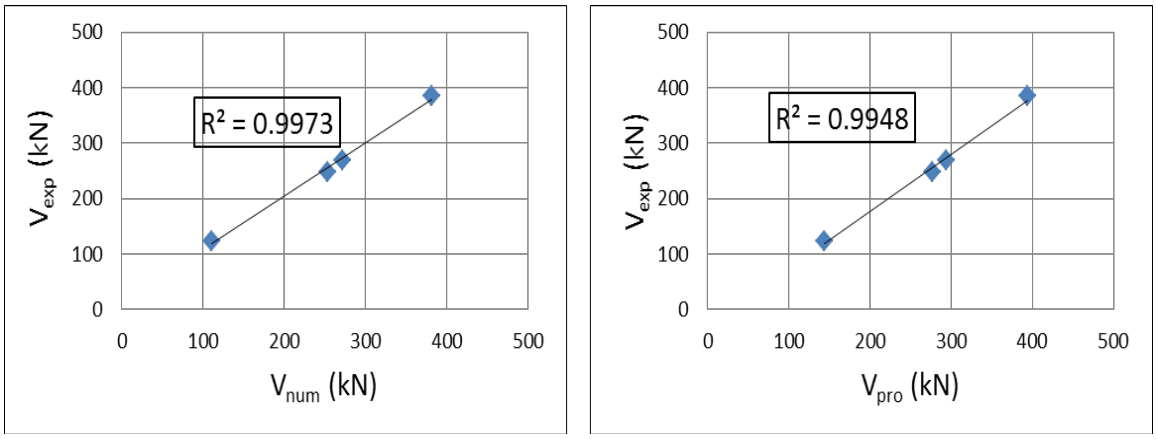

Fig. 5.33: Relationship between experimental, numerical and proposal punching load (Eq.5.2) for the slabs tested at the lab

The above effort was applied to UHPC slabs with steel fibers. To extend this work to include NSC , HSC and UHPC slabs without steel fibers, a modification to Equation 5.2 is made by using the critical perimeter adopted by ACI-318 (b_o = 4(c+d)) as well as matrix tensile strength. Therefore, the final form of Equation 5.2 will be:

$$V_{pro}=0.3[\beta_d\,(v_{fc}+v_{ftm}+v_{\varrho})\,b_o\,d] \qquad \text{.....(5.8)}$$

where;

v_{ftm} is the matrix tensile strength of the NSC slab and the UHPC slab without steel fibers,

$b_o = 4\,(c+d)$; and

c is the column dimension and d is the effective depth of concrete

The application of Equation 5.8 and the ratio of experimental to the proposal values of the NSC slab and the UHPC slab without steel fibers (G1Ufib0 and G2Nfc40) are shown in Table 5.8. A satisfactory prediction can be observed.

Table 5.8: Numerical and proposal punching load (Eq.5.8) for G2Nfc40 and G1Ufib0 slabs

Slab	fiber content	Type of Concrete	V_{exp}	V_{pro}	V_{exp} / V_{pro}
G2Nfc40	0	NSC	169.3	202.1	0.83
G1Ufib0	0	UHPC without steel fiber	210.6	281.6	0.75

5.12 Application of Proposed Design Equation to HSC and NSC Slabs

For further checking of the applicability of the applied modified proposed design Equation 5.8 to NSC and HSC concrete slabs without steel fiber, Equation 5.8 is checked with the test results from earlier research.

The test results from Birkle and Dilger [25], Marzouk and Hussein [30], Elstner and Hognestad [58], Kinnunen and Nylander [61], Muttoni [1] Osman et al. [43] for NSC slabs and Marzouk and Hussein [30], Melo et al. [15], Ghannoum [45], Gardner [48], Elstner and Hognested [58], Marzouk and Jiang [32], Marzouk et al. [27], Adetifa and Polak [7], Osman et al. [43], Hallgren and Kinnuen [47] for HSC slabs were used to check the applicability of Equation 5.8 to NSC and HSC slabs without steel fibers and the results are shown in Table 5.9, Table 5.10, Figure 5.34 and Figure 5.35. For a wide range of slab thickness (90 to 456 mm), column dimensions (120 to 520 mm), reinforcement ratio (0.22% to 3.7%) and compressive strength (12.8 to 108.8 MPa), the modified equation (Equation 5.8) shows unsatisfactory predictions for NSC and HSC slabs with low reinforcement ratio compared with experimental test results.

Table 5.9: Proposed and tested punching loads for NSC slabs

DATA	Slab	h (mm)	c (mm)	ϱ (%)	f_c (MPa)	V_{test} (kN)	V_{pro} (kN)	V_{exp}/V_{pro}
Birkle and Dilger [23]	1	160	250	2.56	33.1	255	478.5	1.00
	7	230	300	2.08	31.4	275	651.9	1.26
	10	300	350	2.16	30	430	836.9	1.25
Marzouk and Hussein [28]	NS1	120	150	1.47	42	408	288.4	1.10
	NS2	150	150	0.94	30	258	317.8	1.24
Elstner and Hognestad [52]	A-1b	150	254	1.15	25.2	258	436.5	0.83
	A-1c	150	254	1.15	29.1	365	441.4	0.80
	A-1d	150	254	1.15	36.8	356	450.6	0.78
	A-1e	150	254	1.15	20.2	352	429.9	0.82
	A-2a	150	254	2.47	13.7	356	439.6	0.75
	A-2b	150	254	2.47	19.5	334	448.0	0.89
	A-2c	150	254	2.47	37.5	400	470.5	0.99
	A-7b	150	254	2.47	28	467	459.1	1.11
	A-3a	150	254	3.7	12.8	512	449.6	0.79
	A-3b	150	254	3.7	22.6	356	463.6	0.95
	A-3c	150	254	3.7	26.6	445	468.8	1.13
	A-3d	150	254	3.7	34.6	534	478.5	1.14
	A-4	150	356	1.15	26.2	547	555.6	0.71
	A-5	150	356	2.47	27.8	400	582.4	0.91
Kinnunen and Nylander [55]	5	151	150	0.8	28.5	534	315.4	0.80
	6	158	150	0.79	27.5	482.3	324.5	0.84
	24	154	150	1.01	28	826.7	323.1	1.33
	25	155	150	1.04	26.7	1046.7	323.8	1.25
	32	156	150	0.49	28	320	314.8	0.81
	33	149	150	0.48	28.3	396	304.8	0.84
Muttoni [1]	PG-1	210	260	1.5	27.6	841	550.9	1.52
	PG-2b	210	260	0.25	40.5	420	524.8	0.80
	PG-4	210	260	0.25	32.2	344	512.9	0.67
	PG-5	210	260	0.33	29.3	455	514.4	0.88
	PG-10	210	260	0.33	28.5	454	513.2	0.88
	PG-11	210	260	0.75	31.5	682	537.4	1.26
	PG-3	456	520	0.33	32.4	1730	1238.3	1.39
	PG-6	96	130	1.5	34.7	231	223.9	1.03
	PG-7	100	130	0.75	34.7	197	222.0	0.88
	PG-8	117	130	0.28	34.7	137	236.4	0.60
Osman et al. [40]	S4	150	250	1.0	36	432	425.4	1.01
	S5	150	250	0.5	38	319	421.8	0.75

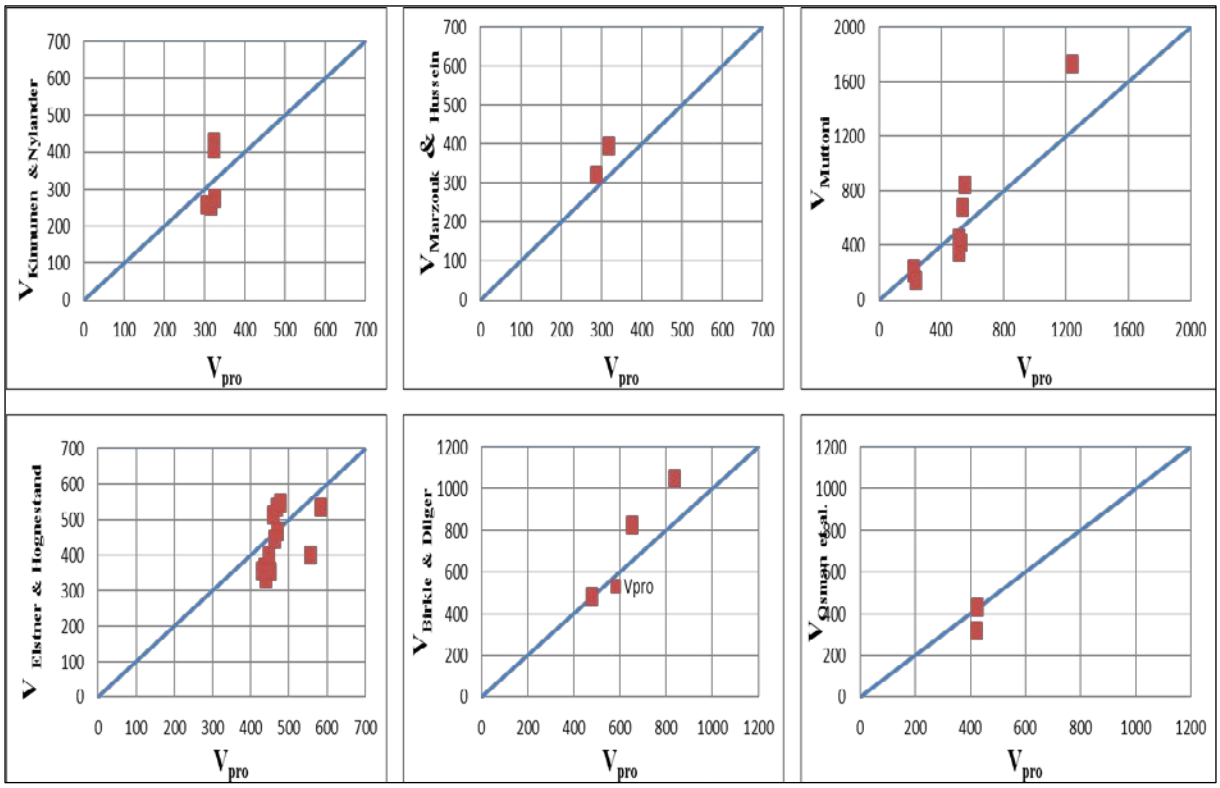

Fig. 5.34: Comparison between proposed (Eq.5.8) and experimental punching load for NSC slabs

Table 5.10: Proposed (Eq.5.8) and tested punching loads for HSC slabs

DATA	Slab	h (mm)	c (mm)	ϱ (%)	f_c (MPa)	V_{exp} (kN)	V_{pro} (kN)	V_{exp}/V_{pro}
Marzouk and Hussein [28]	HS7	120	150	1.193	74	255	306.4	1.16
	HS3	120	150	1.473	69	356	306.3	1.16
	HS4	120	150	2.37	66	356	303.5	1.37
	HS5	150	150	0.64	68	418	342.2	1.06
	HS6	150	150	0.944	70	365	349.6	1.39
	HS8	150	150	1.111	69	489	351.5	1.24
	HS9	150	150	1.611	74	436	361.6	1.50
	HS10	150	150	2.333	80	543	372.9	1.72
	HS1	90	150	0.952	70	645	251.1	0.78
	HS12	90	150	1.524	75	196	259.5	0.99
	HS13	120	150	2	68	258	259.3	1.02
	HS14	120	220	1.473	72	267	396.3	1.25
	HS2	120	300	1.473	71	498	496.0	1.12
Melo et al. [15]	1	118	120	1.5	60.9	560	261.3	1.03
	2	122	120	1.4	62.9	295	267.9	1.25
Ghannoum [42]	S2-U	150	225	0.96	57.1	467	407.6	0.89
	S2-B	150	225	1.92	57.1	538	422.0	1.05
	S3-U	150	225	0.96	67.1	270	416.6	1.06
	S1-U	150	225	1.92	67.1	335	431.0	1.12

Gardner [43]	25	150	180	0.66	66.8	363	374.1	0.81
	27	120	135	1.47	66.8	447	263.3	0.92
	28	120	135	0.45	66.8	443	257.4	0.57
Elstner and Hognested [53]	B-2	150	254	0.476	47.6	485	466.2	1.09
	B-4	150	254	1.01	47.7	306.6	464.6	1.10
	B-9	150	254	2.0	43.9	243	277.4	0.91
	B-14	150	254	3.02	50.5	147.7	306.4	1.16
Marzouk and Jiang	HS 17	150	250	1.0	67	200	306.3	1.16
Marzouk et al. [25]	H.H.Z.S.1.0	150	250	1.0	67.2	334	303.5	1.37
Adetifa and Polak [7]	SB1	120	150	1.2	44	505	342.2	1.06
Abdel Hafez [45]	HS-16	60	100	1.72	63.2	129.5	118.6	1.09
	HS-17	60	100	2.81	63.2	158	121.8	1.29
	HS-18	60	100	2.81	65.6	136	122.3	1.11
	HS-19	60	100	4.24	65.6	160	125.2	1.27
Osman et al. [40]	HSLW 0.5 P	150	250	0.5	76.1	578	461.1	0.65
	HSLW 1.0 P	150	250	1	73.4	511	463.5	1.02
	HSLW 1.5 P	150	250	1.5	75.5	512	474.6	1.13
	HSLW 2.0 P	150	250	2.0	74	253	480.0	1.27
Hallgren and Kinnun-en [46]	HSC 0	125	150*	0.8	90.3	129.5	988.0	0.97
	HSC 1	125	150*	0.8	91	158	989.3	1.03
	HSC 2	125	150*	0.82	85.7	136	963.1	0.92
	HSC 4	125	150*	1.2	91.6	160	1008.4	1.03
	HSC 6	125	150*	0.6	108.8	303.7	1014.1	0.94
	HSC 8	125	150*	0.8	95	473.5	991.1	0.95
	HSC 9	125	150*	0.33	84.1	538.5	947.0	0.60

* diameter of circular column

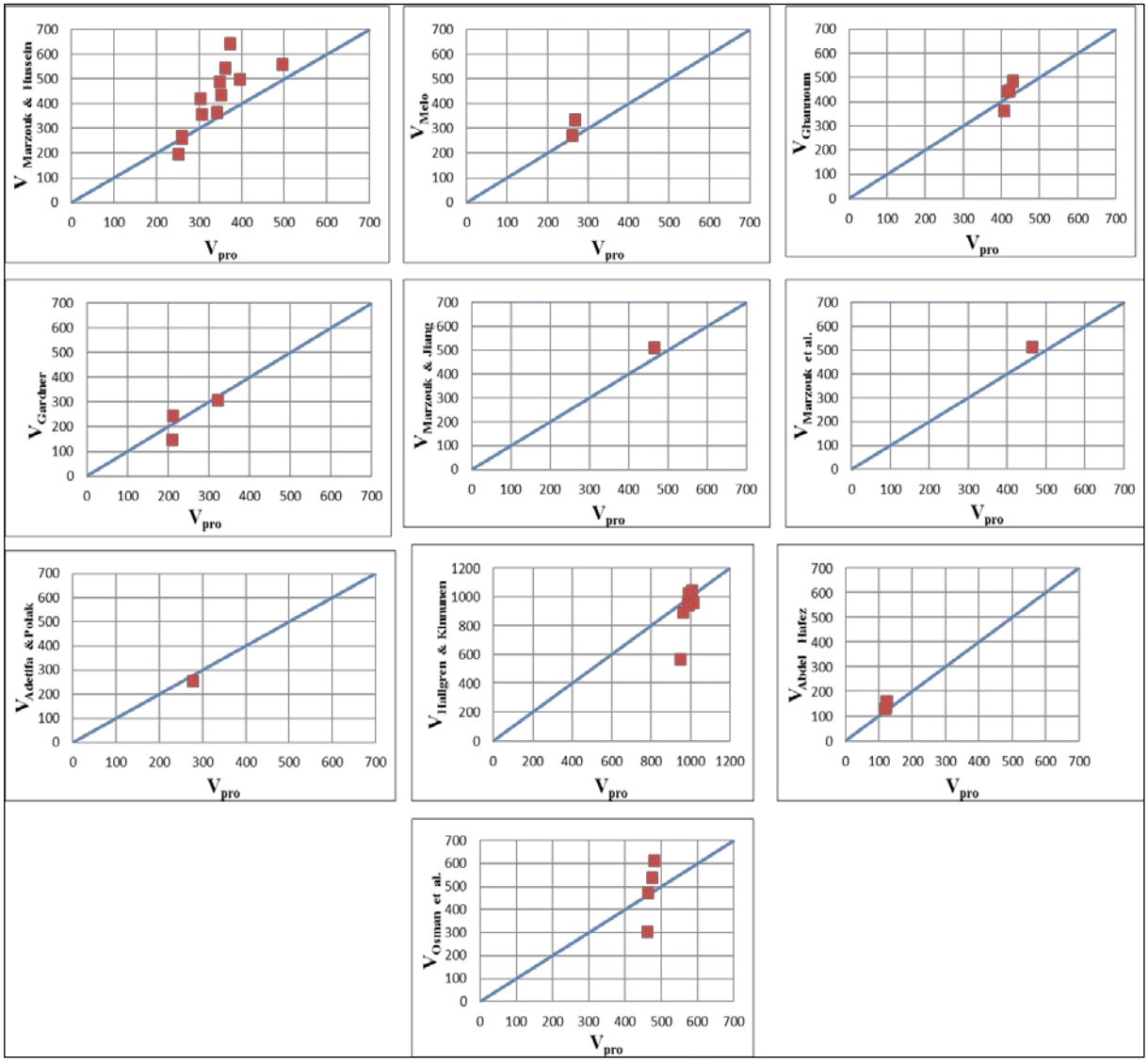

Fig. 5.35: Comparison between proposed (Eq.5.8) and experimental punching load for HSC slabs

Chapter Six

Conclusions and Recommendations

Conclusions

- UHPRC slabs without steel fiber failed by splitting of the concrete cover due to brittle behavior of UHPC and limited tensile strength.

- The post-ultimate load-deformation behavior of UHPC shows three stages of behavior: drop of load-deflection curve after reaching maximum load, resistance of steel fibers and tension reinforcement, and pure tension reinforcement resistance according to geometric nonlinearity.

- As in NSC slabs, an increase of steel fiber content in UHPC slabs will delay the appearance of flexural cracks and increase the first flexural crack load.

- The critical shear crack for UHPC slabs is opened at a load higher than that of NSC slabs.

- The thickness of the slab is a very important factor governing the final shape of the punching cone.

- The diameter of the punching cone for UHPC slabs is larger than that of NSC slabs and the location of critical shear crack at the tension surface is far away from the face of the column. The angle of punching cone of UHPC slabs is less than that of NSC slabs.

- For UHPC, the critical shear perimeter is proposed to be taken at 2.5d from the face of the column, and can be defined as: $b_o = 4c + 5 \pi d$.

- The final shape of the punching cone is completed after the tension reinforcement under the column stub starts to yield and the column stub has penetrated through the slab.

- A numerical model using FEM for UHPC slabs is presented and some variable effects on punching shear capacity were demonstrated by a parametric study.

- A proposed design equation for UHPC under punching load was presented and checked against 62 test results of slabs numerically analyzed and 6 slabs experimentally tested, with conditions ranging from ductile shear failure to

brittle punching failure, from small to high size specimens, from low to high reinforcement ratios and compressive strengths.

- The proposed design equation of UHPC slabs has been modified to apply to HSC and NSC concrete slabs without steel fibers.

Recommendations

For future works, it is recommended to:

- Study the effect of type of steel fiber on punching shear behavior.
- Check the type of failure for UHPC slabs without tension reinforcement (only steel fiber is included).
- Study the size of loading plate as a variable affecting the punching shear behavior of UHPC slabs.
- Study the effect of FRP bars and FRP mesh laminate on punching shear behavior of UHPC slabs.

References

1. A. Muttoni; Punching Shear Strength of Reinforced Concrete Slabs without Transverse Reinforcement; ACI Structural Journal; August 2008.

2. A.G. Sherif and W.H. Dilger; Tests of Full-Scale Continuous Reinforced Concrete Flat Slabs; ACI Structural Journal; June 2000.

3. A.M. Shaaban and H. Gesund; Punching Shear Strength of Steel Fiber Reinforced Concrete Flat Plates; ACI Structural Journal; August 1994.

4. B. Binici and O. Bayrak; Use of Fiber-Reinforced Polymers in Slab-Column Connection Upgrades; ACI Structural Journal; February 2005.

5. B.V. Rangan; Punching Shear Design in the New Australian Standard for Concrete Structures; ACI Structural Journal; April 1990.

6. Boon Tiong; Punching Shear Capacity of Flat Slab-Column Junctions; Thesis of Doctor degree, Department of Civil Engineering University of Glasgow; March 1997.

7. B. Adetifa and M. Polak; Retrofit of slab column interior connections using shear bolts; ACI Structural Journal; 2005.

8. C.E. Broms; Punching of Flat Plates-A Question of Concrete Properties in Biaxial Compression and Size Effect; ACI Structural Journal; June 1990.

9. C.E. Broms; Ductility of Flat Plates: Comparison of Shear Reinforcement Systems; ACI Structural Journal; December 2007.

10. C. Chen and C. Li; Punching Shear Strength of Reinforced Concrete Slabs Strengthened with Glass Fiber-Reinforced Polymer Laminates; ACI Structural Journal; August 2005.

11. C. Cho and M. Park; A 3-D Finite Element Model For R/C Structures Based on Orthotropic Hypoelastic Constitutive Law; KCI Concrete Journal; January 2001.

12. C.E. Ospina, S.D.B. Alexandrer and J.J.R. Cheng; Punching of Two-Way Concrete Slabs with Fiber-Reinforced Polymer Reinforcing Bars or Grids; ACI Structural Journal; October 2003.

13. C.E. Broms; Ductility of Flat Plates: Comparison of Shear Reinforcement System; ACI Structural Journal; December 2007.

14. Cervenka Consulting; ATENA program documentation; Prague, Czech Republic 2009.

15. Cervenka Consulting; ATENA Engineering Examples Manual; Prague, Czech Republic 2009.

16. D. Yitzhaki; Punching Strength of Reinforced Concrete Slabs; Journal of The American Concrete Institute; May1966.

17. D.R. Oliveira, G.S. Melo and P.E. Regan; Punching Strength of Flat Plates with Vertical or Inclined Stirrups; ACI structural Journal; April 2001.

18. D. Tuan Ngo; Punching Shear Resistance of High-Strength Concrete Slabs; Electronic Journal of Structural Engineering; January 2001.

19. D.R.C. Oliveira, P.E. Regan and G.S.S.A. Melo; Punching Resistance of RC Slabs with Rectangular Columns; Magazine of Concrete Research; April 2004.

20. D. Faria, H. Biscaia, V. Lúcio and A.P. Ramos; Material and Geometrical Affecting Punching of Reinforced Concrete Flat Slabs With Orthogonal Reinforcement; fib Symposium; PRAGUE 2011.

21. E. Fehling, T. Leutbecher and F.K. Roeder; Compression-Tension Strength of Reinforced and Fiber-Reinforced Concrete; ACI Structural Journal; May 2011.

22. E. Fehling, T. Leutbecher, R. Friedrich and S. Simomne; Structural behavior of UHPC under biaxial loading; Second international Symposium on Ultra High Performance Concrete; March 2008.

23. E. Fehling and M. Ismail; Expermintelle und Numerische Untersuchungen von Bewehrten UHPC-Bauteilen unter Reiner Torsion; Deutscher Ausschuss für Stahlbeton; 53. Forschungskolloquium; October 2012.

24. G.S.S.A. Melo and P.E. Regan; Post-Punching Resistance of Connections between Flat slabs and Interior Columns; Magazine of Concrete Research; Novemeber 1997.

25. G. Birkle and W.H. Dilger; Influence of Slab Thickness on Punching Shear Strength; ACI Structural Journal; April 2008.

26. G. Jürgen, L. Ludger, E. Christian and W. Maik; Multi-axial and Fatigue behavior of ultra-high-performance concrete (UHPC); Second international Symposium on Ultra High Performance concrete; March 2008.

27. H. Marzouk, M. Emam and M.S. Hilal; Effect of High-Strength Concrete Slab on the Behavior of Slab-column Connections; ACI Structural Journal; June 1998.

28. H. Marzouk and M. Osman and A. Hussein; Punching Shear of Slabs: Crack Size and Size Effects; Magazine of Concrete Research; February 2002.

29. H. Al-Quraishi and E. Fehling; Punching Shear Behavior of UHPC Flat Slabs; 53. Forschungskolloqium; Oktober 2012.

30. H. Marzouk and A. Hussein; Experimental Investigation on the Behavior of High-Strength Concrete Slabs; ACI Structural Journal; December 1991.

31. H.M. Marzouk and Z. Chen; Finite Element Analysis of High-Strength Concrete Slabs; ACI Structural Journal; October 1993.

32. H.M. Marzouk and D. Jiang; Experimental investigation on shear enhancement types for high-strength concrete plates; ACI Structural Journal 1997.

33. H. Higashiyama, A. Ota, and M. Mizukoshi; Design Equation for Punching Shear Capacity of SFRC Slabs; International Journal of Concrete Structures and Materials; June 2011.

34. H. Park and E.H. Kim; RC Flat Plate under Combined In-Plane and Out-of-Plane Loads; Journal of Structural Engineering; October 1999.

35. Joo-HaLee, Young-Soo Yoon, W.D. Cook and D. Mitchell; Improving Punching Shear Behavior of Glass Fiber-Reinforced Polymer Reinforced Slabs; ACI Structural Journal; August 2009.

36. J.S. Kuang and C.T. Morley; Punching Shear Behavior of Restrained Reinforced Concrete Slabs; ACI Structural Journal; February 1992.

37. J.S. Lovrovich and D.l. McLean; Punching Shear Behavior of Slabs with Varying Span-Depth Ratios; ACI Structural Journal; Septemeber 1990.

38. J. Lee, Y. Yoon, W.D. Cook and D. Mitchell; Improving Punching Shear Behavior of Glass Fiber-Reinforced Polymer Reinforced Slabs; ACI Structural Journal; August 2009.

39. J.L. Clarke and F.K. Birjandi; Punching Shear Resistance of Lightweight Aggregate Concrete Slabs; Magazine of Concrete Research; September 1990.

40. K.V. Papanikolaou, I.A. Tegos and A.J. Kappos; Punching Shear Testing of Reinforced Concrete Slabs, and Design Implications; Magazine of Concrete Research; April 2005.

41. K. Sissakis and S.A. Sheikh; Strengthening Concrete Slabs for Punching Shear With carbon Fiber-Reinforced Polymer Laminates; ACI Structural Journal; February 2007.

42. L. Moreillon, J. Naseir and R. Suter; Shear and Flexural Strength of Thin UHPC Slabs; Proceedings of Hipermat; Kassel March 2012.

43. M. Osman, H. Marzouk and S. Helmy; Behavior of High-Strength Lightweight Concrete Slabs under Punching Loads; ACI Structural Journal; June 2000.

44. M. di Priscoo and R. Felicetti; Some Results on Punching Shear in Plain and Fiber-Reinforced micro-Concrete Slabs; Magazine of Concrete Research; September 1997.

45. M. Ghannoum; Effect of high strength concrete on the performance of the column-slab specimens; MSc. Thesis; McGill University; Canada 1998.

46. M. Abdel Hafez; punching shear behavior of normal and high-strength concrete slabs under statics loading; Journal of Engineering Sciences; 2005.

47. M. Hallgren and S. Kinnunen; Increase of punching shear capacity by using high-strength concrete; 4th International Symp. On Utilization of high strength concrete; Paris 1996.

48. N.J. Gardner; relationship of the Punching Shear capacity of Reinforced Concrete Slabs with Concrete Strength; ACI Structural Journal; February 1990.

49. P.E. Regan; The dependency of punching resistance upon the geometry of the failure surface; Magazine of Concrete Research; Vol.36, No.126, March 1984.

50. P.E. Regan; Symmetric punching of reinforced concrete slabs; Magazine of Concrete Research; Vol.38, No.136; September 1986.

51. P.J. McHarg, W.D. Cook, D. Mitchell and Y. Soo Yoon; Benefits of Concentrated Slab reinforcement and Steel Fibers on Performance of Slab-Column Connections; ACI Strucrural Journal; April 2000.

52. P. Menêtery; Relationships between Flexural and Punching Failure; ACI Structural Journal; August 1998.

53. P.S. Baglin and R.H. Scott; Finite Element Modeling of Reinforced Concrete Beam-Column Connections; ACI Structural Journal; December 2000.

54. Qi Zhang; Finite Element Application to Slab-Column Connections Reinforced with Glass Fiber-Reinforced Polymers; Memorial University of Newfoundland; April 2004.

55. R.B. Gomes and P.E. Regan; Punching Resistance of RC Flat Slabs with Shear Reinforcement; Journal of Structural Engineering; June 1999.

56. R. Narayanan and I.Y.S. Darwish; Punching Shear Tests on Steel-Fiber Reinforced Mico-Concrete Slabs; Magazine of Concrete Research; March 1987.

57. R. Narayan and I.Y.S. Darwish; Use of Steel Fibers as Shear Reinforcement; ACI structural Journal; June 1987.

58. R. Elstner and E. Hognestad; Shearing Strength of Reinforced Concrete Slabs; ACI Journal Proceeding; Feb. 1956.

59. S. Teng, H.K. Cheong, K.L. Kuang and J.Z. Geng; Punching Shear Strength of Slabs with Opening and Supported on Rectangular Columns; ACI Structural Journal; October 2004.

60. S.D.B Alexander and S.H. Simmonds; Punching Shear of Concrete Slab-Column Joints Containing Fiber Reinforcement; ACI Structural Journal; August 1992.

61. S. Kinnunen and H. Nylander; Punching of Concrete Slabs Without Shear Renforcement; Transctions, Royal Insitute of Technology, Stockholm; March 1960

62. Widianto, O. Bayrak and J.O. Jirsa; Two-Way Shear Strength of Slab-Column Connections: Reexamination of ACI 318 Provisions; ACI Structural Journal; April 2009.

63. W. Kolmar; Beschreibung der Kraftübertragung über Risse in nichtlinearen Finite Element Berechnungen von Stahlbetontragwerken; Thesis, TU Darmstadt, Darmstadt 1985.

64. W. Salim and W.M. Sebastian; Punching Shear Failure in Reinforced Concrete Slabs with Compressive Membrane Action; ACI Structural Journal; August 2003.

65. Y. Tian, J.O. Jirsa and O. Bayrak; Strength Evaluation of Interior Slab-Column Connections; ACI Structural Journal; December 2008.

66. Y. Tian, J.O. Jirsa, O. Bayrak, Widianto and J.F. Argudo;Behavior of Slab-Column Connections of Existing Flat-Plate Structure; ACI Structural Journal; October 2008.

67. Y.S. Cho; Structural Performance of RC Flat Plate Slab Shear-Reinforced Interior Connections Under lateral Loading; Magazine of Concrete Research; April 2009.

68. Y. Loo and H. Guan; Cracking and Punching Shear Failure Analysis of RC Flat Plates; Journal of Structural Engineering; October 1997.

69. Z.P. Bažant and Z. Cao; Size Effect in Punching Shear Failure of Slabs; ACI Structural Journal; February 1987.

List of Figures

List of Tables

Appendix

Mix Design for all Tested Slabs

1. Compositions of M3Q for G1Ufib0 (UHPC of 0% fiber content) were presented in Table A.1-1.

Table A.1-1: Composition of G1Ufib0 slab

Material	Weight (Kg)
Water	18.39
portland cement	86.72
Silica fume	18.39
Superplasticizer	3.28
fine quarz	21.02
sand 0.125/0.5	102.48
steel fiber	0.00

2. Compositions of M3Q for G1Ufib0.5 (UHPC slab with 0.5% steel fiber) were presented in Table A.1-2.

Table A.1-2: Composition of G1Ufib0.5 slab

Material	Weight
Water	18.30
portland cement	86.28
Silica fume	18.30
Superplasticizer	3.26
fine quarz	20.91
sand 0.125/0.5	101.96
steel fiber (0.25mm/20mm)	4.16

3. Compositions of M3Q for G1Ufib1.1 (UHPC with 1.1% steel fiber) were presented in Table A.1-3.

Table A.1-3: Composition of G1Ufib1.1slab

Material	Weight(kg)
Water	18.19
portland cement	85.75
Silica fume	18.19
Superplasticizer	3.24
fine quarz	20.78
sand 0.125/0.5	101.34
steel fiber (0.25mm/20mm)	9.15

4. Compositions of normal strength concrete slab were presented in Table A.1-4.

Table A.1-4: Composition of normal strength concrete slab

Material	Weight(kg)
Water	20.15
portland cement	32.73
Sand 0/2	76.7
Gravel 2/16	73.53
Water / cement ratio	61.5%

5. Compositions of M3Q for G1Uϱ1% (UHPC with 1% reinforcement ratio) were presented in Table A.1-5.

Table A.1-5: Composition of G3Uϱ1% slab

Material	Weight (kg)
Water	18.30
portland cement	86.28
Silica fume	18.30
Superplasticizer	3.26
fine quarz	20.91
sand 0.125/0.5	101.96
steel fiber (0.25mm/20mm)	4.16

6. Compositions of M3Q for G4Ut55 (UHPC with 55mm thickness) were presented in Table A.1-6.

Table A.1-6: Composition of G4Ut55 slab

Material	Weight (kg)
Water	8.63
portland cement	40.69
Silica fume	8.63
Superplasticizer	1.54
fine quarz	9.86
sand 0.125/0.5	48.09
steel fiber (0.25mm/20mm)	1.96

7. Compositions of M3Q for G5Ufy560 (UHPC with normal yield stress tension bars) were presented in Table A.1-7.

Table A.1-7: Composition of G5Ufy560 slab

Material	Weight (kg)
Water	18.30
portland cement	86.28
Silica fume	18.30
Superplasticizer	3.26
fine quarz	20.91
sand 0.125/0.5	101.96
steel fiber (0.25mm/20mm)	4.16

Zusammenfassung

Am Institut für Konstruktiven Ingenieurbau des Fachbereichs Bauingenieur- und Umweltingenieurwesen der Universität Kassel wurden Reihenuntersuchungen von Verbindungen zwischen Stützen und Decken durchgeführt, um das Durchstanzverhalten von Flachdecken zu untersuchen.

Die Auswirkungen des Stahlfasergehalts, der Betondruckfestigkeit, des Bewehrungsgrades und der Streckgrenze der Stabstahlbewehrung wurden in Tests an insgesamt sechs UHPC-Platten und einer Platte aus normalfesten Beton untersucht.

Die experimentellen Ergebnisse belegen ein Versagen aller Platten durch Durchstanzen, mit Ausnahme der UHPC-Platte ohne Stahlfasern, welche durch Abspaltung der Betondeckung versagte. Die Lastverformungskurve im Nachbruchbereich der UHPC-Platten weist ein duktiles Verhalten in drei Bereichen auf. Erstens zeigt sich ein Abfall der Lastverformungskurve nach Erreichen der Maximallast, zweitens ein duktiles Verhalten durch Aktivierung der Stahlfasern und der Stabstahl-Bewehrung und drittens die alleinige Wirkung der Stabstahl-Bewehrung.

Der erste Schub-Riss der UHPC-Platten beginnt sich erst bei einer Belastung zu öffnen, die höher liegt als die der Platte aus normalfestem Beton (NSC). Typischerweise ist der Durchmesser des Durchstanzkegels für UHPC-Platten auf der Zugseite größer als der von NSC-Platten.

Der Winkel zwischen der Stabstahl-Bewehrung und dem Durchstanzkegel für NSC-Platten ist größer als der für UHPC-Platten. Für UHPC-Platten wird vorgeschlagen, den kritischen Umfang bei einem Abstand von 2,5 d von der Stützeninnenkante zu wählen. Die endgültige Form des Ausbruchskegels zeigt sich nach dem Fließen der Stabstahl-Bewehrung und dem Einsinken des Stützenquerschnitts in die Platte.

In der vorliegenden Arbeit wurde ein numerisches Modell für UHPC-Platten unter Zuhilfenahme der Finite-Element-Analyse verwendet. Durch eine Parameter-Studie wurde der Einfluss einiger Variablen auf das Durchstanzen untersucht.

Eine Bemessungsgleichung für UHPC-Platten unter Durchstanzen wurde vorgestellt und ihre Anwendbarkeit für eine Vielzahl von Parametervariationen untersucht: für Plattenstärken von 40 mm bis 300 mm, für Stabstahl-Bewehrungsgrade von 0,1 % bis 2,9 %, für Betondruckfestigkeiten von 150 MPa bis 250 MPa und Stahlfasergehalten von 0,1 % bis 2 %. Die vorgestellte Bemessungsgleichung der UHPC-Platten wurde für die Anwendung an (hochfesten) HSC- und (normalfesten) NSC-Platten ohne Stahlfasern modifiziert, und an Testergebnissen aus früheren Untersuchungen verifiziert.